



Review

Lilong Dai, Zinan Huang, Qianqian Huang, Chang Zhao, Aleksey Rozhin, Sergey Sergeev, Mohammed Al Araithi and Chengbo Mou*

Carbon nanotube mode-locked fiber lasers: recent progress and perspectives

<https://doi.org/10.1515/nanoph-2020-0446>

Received August 4, 2020; accepted August 25, 2020;

published online November 24, 2020

Abstract: Carbon nanotubes (CNTs) possess remarkable nonlinear optical properties; a particular application is to function as a mode locker used in ultrafast fiber lasers to produce ultrashort optical pulses. Various types of CNT saturable absorbers (SAs) and ultrafast fiber lasers have been demonstrated. In this review, typical fabrication process and development of CNT SAs are discussed and we highlight the recent investigation and progress of state-of-the-art ultrafast fiber lasers covering GHz, bidirectional ultrafast fiber lasers, vectorial mode fiber lasers, comb systems, and mode-locking dynamics. Our perspectives of ultrafast fiber lasers based on CNT SAs are given finally.

Keywords: carbon nanotubes; frequency comb; mode-locked fiber lasers; nanomaterials; ultrafast photonics.

1 Introduction

In the past few decades, ultrafast fiber lasers have gained enormous attention and found applications covering broad fields from fundamental research to industrial process,

based on their salient advantages, including maintenance-free operation, compactness, cost-effective design, high beam quality, high-efficient heat dissipation and rather low price [1–3]. The diversity of rare-earth-doped fiber gain medium is identified as a key element in the fiber resonator cavity and essential to produce various operation wavelengths ranging from near infrared to mid infrared [4–7]. Typically, commercial ultrafast fiber laser systems dominate in 1.55 and 1.06 μm for great demand in communication and industrial applications. Other wavelengths that are sensitive to different molecules may have potential in establishment of precise monitoring systems [8]. Especially, molecular absorption in 2 μm and beyond plays significant roles in medical surgery [9].

Ultrashort pulses are generally produced by inserting a nonlinear optical element into a resonator cavity as an intensity discriminator, which is called a saturable absorber (SA). The basic function of SA is to suppress low incident intensity beam while support higher intensity spikes and the working mechanism has been revealed in other Ref [10]. Typical demonstrated SAs in ultrafast fiber lasers include nonlinear polarization rotation [11, 12], nonlinear optical loop mirror [13], and nonlinear amplifying loop mirror (NALM) [14]; semiconductor saturable absorber mirrors (SESAMs), carbon nanotubes (CNTs) [15, 16], graphene [17], topological insulators [18, 19], transition metal dichalcogenides [20–23] and black phosphorus [24–28], MXenes [29, 30], bismuthine [31–33] and antimonene [34, 35], perovskite [36–38], gain medium [39], nonlinear multimodal interference effect [40], alcohol [41], pure water [42], metals [43], quantum dots [44, 45], etc.

CNTs possess multiple excellent properties and advantages that are well fitted with the requirements of a good SA. The measured third-order nonlinear polarizability by pump probe spectroscopy is 10^{-7} – 10^{-10} esu (1 esu = 1.11×10^{-9} m² V⁻²) [46]. The recovery time was measured to be composed with a fast intraband carrier relaxation time of 0.3–1.2 ps and a slow recombination process of 5–20 ps [47]. Moreover, the superior thermal conductivities as high as 5000 W m⁻¹ guarantee intrinsic

*Corresponding author: **Chengbo Mou**, Key Laboratory of Specialty Fiber Optics and Optical Access Networks, Shanghai Institute for Advanced Communication and Data Science, Joint International Research Laboratory of Specialty Fiber Optics and Advanced Communication, Shanghai University, Shanghai, 200444, P. R. China, E-mail: mouc1@shu.edu.cn. <https://orcid.org/0000-0001-6107-3439>

Lilong Dai, Zinan Huang, Qianqian Huang and Chang Zhao, Key Laboratory of Specialty Fiber Optics and Optical Access Networks, Shanghai Institute for Advanced Communication and Data Science, Joint International Research Laboratory of Specialty Fiber Optics and Advanced Communication, Shanghai University, Shanghai, 200444, P. R. China

Aleksey Rozhin and Sergey Sergeev, Aston Institute of Photonic Technologies (AIP), Aston University, Birmingham, B4 7ET, UK

Mohammed Al Araithi, Higher College of Technology, PO Box 74, Postal Code 133, Al-Khufair, Sultanate of Oman

high-power handling. Mature growth process greatly reduces the price of raw materials and meanwhile research cost. More importantly, the development of CNT SAs over the past 15 years clear the path to all-fiber integration configuration, and extensive studies have verified its broad operation wavelength range which is an intrinsic drawback of commercial SESAMs. Thus, CNT SAs have confidence to perform as a promising substitution to SESAMs in the future.

The first verification of CNTs as SA in ultrafast fiber laser system took place in 2003 by Set et al. and ultrashort pulses of ~ 1 ps was demonstrated in 1550 nm [48]. CNT SAs have subsequently been rapidly adopted by many research groups and until now. The development of CNT SAs based on fiber laser may be summarized as: (1) The initial demonstration of CNT SAs for different gain medium, operation wavelength, operation states (*Q*-switching, mode locking) to ensure the feasibility; (2) In view of the superior properties as an SA, effective modification of cavity design gains more interests including wavelength-tuning, wavelength-switching, multiwavelength, pulse-shaping regime switching, etc. These phenomena assure the stability and compatibility of CNT SAs; (3) The recent cases pay more attention to advanced applications and research platforms as physical mechanism. There are some review articles focusing on the nonlinear optical properties and the success as SAs for ultrafast laser pulses [10, 49–51].

Compared with commercial fiber lasers, the biggest challenges of CNT mode-locked fiber lasers met mainly come from energy and stability. Broad operational wavelength range has been confirmed previously. The intrinsic high-power handling of CNT ensures the possibilities to generate high-energy pulses and mature chirped pulses amplification technique is able to produce commercial-grade energy pulses. Generally speaking, a stable and high-power fiber laser seed based on a CNT SA is a must. Based on such considerations, various attempts have been applied from CNT SAs side and laser configuration side, including environment-friendly polymer selection, freestanding CNT film, interaction with evanescent field, all-polarization-maintaining fiber configuration, antivibration treatment, etc.

This study will emphasize more on the state-of-the-art ultrafast fiber lasers based on CNT mode locker, including the fabrication and characteristics of a CNT SA, especially detailed dispersion theory, Raman mapping results and uniformity, stability discussion. Such comments are aimed to improve the fiber laser performance on the CNT SAs side. Besides, recent progress and applications of CNT-based ultrafast fiber laser is highlighted, involving GHz fiber

lasers, comb systems, vectorial mode fiber lasers, bidirectional mode-locked fiber lasers and mode-locking dynamics of fiber lasers. Finally, conclusions and perspectives are given.

2 Fabrication and characteristics of CNT SAs

2.1 Selection of CNTs

Commercial CNT powders can be produced by several processes, including arc discharge (AD), laser ablation (LA), chemical vapor deposition (CVD), high-pressure carbon monoxide reaction (HiPco), and cobalt and molybdenum catalyst process (CoMoCAT). The construction of AD consists of a reaction chamber full of medium (inert gas or liquid) containing a pair of carbon electrodes (anode and cathode) with small distance of 1–2 mm from each other and the diameter of them is on the level of millimeters while the anode is usually smaller than the cathode. The reaction procedure starts from the current promote electrode to heat up to 4000–5000 K and result in ionization of surrounding medium as well as plasma formation between electrodes. The high temperature of anode sublimates carbon and evaporates it; besides, the high energy accompanied with the medium leads to disruption of carbon vapors and carbon ions formation.

The synthesis process of LA is typically based on a YAG or CO₂ laser beam, where the intense laser pulses ablate the graphite target which is placed into a furnace heated to 1200 °C in the presence of an inert gas (helium, argon or nitrogen). The carbon vapors are then directed toward the cold collector as the gas flows.

Compared with the AD and LA, CVD technique is the most promising technique for possible industrial application due to the relative low operation temperature (600–1200 °C), high purity and high yield. In CVD, the synthesis of CNTs is processed by decomposition of hydrocarbon vapor over the catalyst particle or without a catalyst. When the CNT precursor is vaped and the vapor is contacted with heated metal catalyst, it is first decomposed into carbon and hydrogen. Hydrogen leaves with the passing carrier gas or reducing gas, whereas the carbon dissolves in the metal catalyst. When the temperature reaches the carbon solubility limit of the metal, the decomposed carbon particles precipitate and crystallize to form CNTs. Based on different interactions between the catalyst and the substrate, such growth mechanism can be

concluded as two parts: *tip growth* and *root growth*. Besides, its derivatives can be widely used to grow vertically aligned CNTs and allows more chirality controlling.

The HiPco process is a gas-phase process that uses the floating catalyst approach, whereby the catalytic particles are formed in situ by thermal decomposition of the catalyst precursor ($\text{Fe}(\text{CO})_5$). CNTs from HiPco are formed from the CO disproportionation over iron particles in accordance with the Boudouard reaction. The iron particles are decomposed from the catalyst precursor and act as growth nucleation site, where CNTs are grown around the catalyst cluster. Another attractive alternative to the CVD processes is the catalytic decomposition of a carbon-containing molecule on substrate-supported catalyst particles (Co and Mo). The synthesis process of CoMoCAT is similar to HiPco, whereas the metal catalytic particles are formed from metal Co after Mo oxides are transformed into Mo carbides. This process involves the detailed characterization of the different phases in the catalyst preparation stage to ensure selective production of CNTs.

These growth processes have been reviewed elsewhere [52–58] and the results turn to be that HiPco and CoMoCAT methods are more favorable due to mass production, high purity, and small diameter distribution. In terms of the ratio of semiconductor CNTs (*s*-CNTs) to metallic CNTs (*m*-CNTs), the samples produced from CoMoCAT method tend to own a smaller value but less controllable. Of course, there are some study focusing on the growth of specific chirality of CNTs [59–62] and this can be used to study the effect on final SA characteristics and laser performances from the aspect of carbon source.

CNTs as good SAs have been widely demonstrated in various types of ultrafast fiber laser systems. However, the output characteristics and inherent dependency on diversity of SAs do exist. The principle of how to choose a suitable CNT as a desirable SA for the desired laser performance is still under investigation.

In terms of geometrical construction, CNTs can be divided into single-walled CNTs (SWNTs), double-walled CNTs (DWNTs) and multiwalled CNTs (MWNTs). An SWNT consists of a single graphene layer rolled into a seamless cylinder, whereas DWNTs and MWNTs are composed of two and more concentric cylindrical graphene shells coaxially arrayed around a central hollow core and separated with van der Waals forces between adjacent layers. In addition to SWNTs which are proved to be a superior SA, DWNTs and MWNTs have also been verified to be able to produce short pulses, either from mode locking or from *Q*-switching, in a broad operation wavelength range [63–65]. They do possess some advantages compared with SWNTs: relatively simple production environment and

condition, as well as low production cost and 50–80% cheaper price; higher thermal stability which result in higher damage threshold and development of higher power lasers; greater photon absorption characteristics and environmental stability. However, the saturable intensity for MWNTs with outer diameter of 40 nm reach a high level of 100 GW/cm^2 much larger than SWNTs, and MWNTs may have outer and inner wall combination with different electronic types (*s*–*m*, *s*–*s*, *m*–*m*). Such structures complicate the nonlinear optical properties of SAs meanwhile extremely hard to control during fabrication. Hence, SWNTs are still more favorable than DWNTs and MWNTs in ultrafast lasers experiment based on considerable exploration. In this review article, we will focus on SWNTs as SAs, including selection, dispersion, characterizations and applications in ultrafast fiber lasers.

As described previously, many methods have been applied to produce SWNTs, but there are still considerable impurities involved in the final products. This may influence the optical properties and increase the scattering loss, meanwhile weaken the SA effect. High purity of SWNT powder is a must for high-quality SAs. Existence of *s*-SWNTs plays a significant role in the function of a SA. Owing to the typical semiconductor characteristic, optical absorption at a given wavelength produces electron–hole pairs. A higher incident power will lead to conduction band filling or valence band depleting, as well as photo-bleaching, due to Pauli blocking principle [66]. This is also called absorption saturation. The samples we used nowadays are always a mixture of *s*-SWNTs and *m*-SWNTs, where *m*-SWNTs offer a fast relaxation channel for the excited state to guarantee ultrafast recovery time. Moreover, the absorbed wavelength corresponding to the band gap energy usually decides the final operation wavelength. For example, the SWNT SAs operating in near-infrared spectral range is usually related to the first and second band gap in *s*-SWNTs (commonly labeled as S_{11} , S_{22}) [67, 68], truly metallic armchair SWNTs ($n = m$) are zero band gap materials while zigzag *m*-SWNTs ($n - m = 3q$, where q is a nonzero integer) have a very small band gap inversely proportional to the square of the tube radius. In addition, armchair nanotubes packed in bundles have large pseudogaps [69]. The *m*-SWNTs are responsible for the optical absorption mainly in the visible spectral range (labeled as M_{11}), but the optical absorption with energy lower than the van Hove singularities is also possible due to the excitation effects [70] and hot Dirac fermions [71]. Recently, some investigations show that SA implemented by pure *s*-SWNTs or *m*-SWNTs could obtain good laser characteristics [72–74]. Extremely strict growth environment or complicated follow-up treatment [75–83] makes

the cost ultrahigh (75 times or higher) than the original SWNTs powder, such conditions somehow limit its applications. Practically, the choice of a mixture is favorable. However, the ratio of *s*-SWNTs to *m*-SWNTs is also an influential point needed to be considered and require the assistance of development of specific chirality SWNTs growth technique.

Apart from purity and chirality selection of SWNTs, diameter distribution is also an important factor affecting the laser performance and operation condition. First, saturable absorption at a specific wavelength depends on the tube diameter and keeps proportional relationship. For instance, the SWNTs with a diameter range of 0.8–1.3 nm are suitable for application in communication band because they have an absorption band which corresponds to 1300–1600 nm [84]. It is essential to match absorption spectra with the operation wavelength. SWNTs acting as an SA can also be realized at other wavelengths away from the peak resonance where they have appreciable optical absorption. Second, the nonlinear optical properties of SWNT SAs are determined by the saturable absorption resonance with the incident wavelength, so the number of such type of tubes is an important factor. Narrow diameter distribution and sharp absorption peak may enhance nonlinear optical properties and decrease the saturated light intensity or the threshold of mode locking. Certainly, increasing the loading of SWNTs as well as concentration in the final products can reduce the saturation power, but meanwhile, catalysts and amorphous carbon content may increase, this leads to more nonsaturable absorption loss.

2.2 Dispersion of CNTs

Individual or isolated SWNTs own superior nonlinear optical absorption as an SA. However, such excellent performances are restricted by the fact that pristine SWNTs have the tendency to spontaneously agglomerate into large bundles or ropes in the form of an entangled state. This phenomenon arises from several reasons: the high surface area of SWNTs leads to strong attraction force between tubes; high aspect ratios combined with high flexibilities cause easy aggregation and entanglement; the van der Waals attraction energy as high as 500 eV/ μm of tube–tube contact in highly close-packed bundles increases the dispersing difficulty [85–87]. Moreover, SWNTs are considered insoluble in all known solvent. These will weaken electrical, optical, thermal, mechanical properties, so the preparation of effective dispersion of SWNTs in different

solvent and polymer matrix presents a major premise to extension and utilization of SWNTs in ultrafast fiber laser systems. Dispersion of SWNTs in different solvent medium features various methods, from physical treatment to surface modification. There are already several reviews describing this [88–94]; here, we will pay attention to some typical approaches utilized to fabricate CNT SAs.

Ultrasonication is often used to disperse SWNTs in aqueous solution and has been proved to be the most promising and effective technique to obtain good dispersion. Large SWNT bundles in the solvent are separated by the energy transferred from ultrasound wave through the medium. The provided sonication energy is important for the final quality of the dispersed samples; therefore, the sonication energy applied should be able to overcome the binding energy of CNT aggregates but less than the amount required to fracture a tube to maintain the morphology of individual SWNT [91]. Hence, research reveals that the optimal sonication energy depends on the tube diameter rather than the amount of SWNTs or surfactant, surface functional groups and SWNT length [95]. Nowadays, the most effective ultrasonication type is based on ultrasonication probe (tip).

The operation mechanism can be expressed as following: the probe will shock at a certain frequency meanwhile forming a conical field in the solvent. This is responsible for the nucleation and collapse of bubbles. Shear force is created by such process and dominates the separation of SWNT bundles. The wand tip vibrations along with the rapid generation and collapse of bubbles will introduce a flow recirculating between the probe and the forming conical field to enhance the dispersion effect [90, 96]. Several factors can affect the area of conical zone and local velocity field, including boiling point, relative viscosity of solvent, sonication energy, structure of cell and location of probe. To be summarized, lower boiling point, lower viscosity, higher sonication energy and specific cell can improve the circulation efficiency and the rate at which bubbles are generated and collapsed, further promote dispersion quality.

The result of the probe-like ultrasonication configuration is that substantial heat can be generated rapidly; thus for some volatile solvent, such as ethanol and acetone, fast evaporation will weaken the dispersing ability; besides, the increased temperature will enhance the Brownian motion giving large collision probability of separated SWNTs to form bundles again. Hence, the samples normally require external temperature control. Moreover, the sonication process must be operated in short intervals.

2.2.1 Surfactants and aqueous solutions

The entire dispersion process of SWNTs in aqueous solutions majorly contains two parts, dispersion and stabilization. Simple ultrasonication process will offer shear force to obtain effect of disperse. However, the van der Waals attractions between tubes do exist and will lead to re-aggregation. Hence, in the real process of making SWNT SAs, the combination of ultrasonication and noncovalent surface modification is always applied. In accordance with different polymer matrix, dispersion medium can be classified as aqueous solution and organic solvents.

In aqueous solution, surfactants are widely utilized as dispersant to separate SWNTs and they are demonstrated to be one of the simple and most effective ways to nondestructively enhance the dispersibility. The most significant reason of surfactants with such function is an amphiphilic molecule structure, which possesses a hydrophobic head group attached to the side walls of tube and a hydrophilic tail interacted with the polar solvent [97, 98]. Surfactants can be divided into three main classes: ionic (anion (sodium dodecylbenzene sulfonate (SDBS) [99], sodium dodecyl sulfate (SDS) [100, 101], sodium tetradecylsulfate (STDS/STS) [101], sodium cholate [102], sodium deoxycholate [103], lithium dodecyl sulfate [104], sodium taurodeoxycholate [105], Dowfax surfactant [106], etc.), cation (dodecyl trimethyl ammonium bromide (DTAB) [97, 101, 107], cetyltrimethyl ammonium 4-vinylbenzoate [108], cetyltrimethylammonium bromide (CTAB) [97, 101, 107], cetyltrimethyl ammonium chloride [90], tetradecyltrimethylammonium bromide (TTAB) [101], cetylpyridinium chloride (CPyCl) [101, 105], etc.) and nonionic (Triton X series [97, 107], Pluronic series [109], Igepal, Brij series [97, 107], Tween series [110], polyoxyethylene 8 lauryl [111], Tergitol NP-7 [112], etc.). The ionic surfactants are more favorable and effective in aqueous solvent, whereas nonionic surfactants are more suitable for organic solvent. The use of surfactants is usually combined with ultrasonic treatment and it is revealed that shear forces applied on CNTs play a more critical role than the surfactant. The dispersion process, also

called unzipping mechanism, can be approximately described in Figure 1A [113, 114]: high local shear force generated by cavitation process mainly acts from head of close-packed CNT bundles, once the van der Waals force between tube–tube interaction is defeated, some small gaps will appear and the surfactants will attach CNTs by hydrophobic adsorption or π - π stacking [91]; this is the origin of dispersion procedure and larger surfactant molecules may show inefficiency in dispersion. As ultrasonic treatment recirculates and the concentration of surfactant reaches critical micelles concentration, the surfactant molecules will assembly into a micelle and adsorb the tube walls in the form of structureless random adsorption (Figure 1B) to achieve good disperse and stable states [115, 116]. There are several factors affecting dispersive efficiency based on structures of surfactants and have been discussed elsewhere [106, 110]. Some research compared a series of surfactants and revealed that SDBS was the best dispersant for CNTs. There is also an order: SDBS > CTAB \approx CPyCl > STS > TTAB \approx SDS > DTAB [101].

However, on removal of the high shear force, the van der Waals between individual CNTs would assemble themselves to a new equilibrium state of low energy, through reaggregation process. The stability is preserved by electrostatic or steric repulsion [91]. Such effect directly depends on the charge of adsorbed groups as well as ionic or nonionic. This can also be determined by the zeta-potential measurement of SWNTs in solvent. If ionic surfactant is used or absolute value of measured zeta-potential is much larger than zero, the dispersion is stabilized by electrostatic repulsion; by contrast, steric repulsion dominates for nonionic surfactant and relatively small zeta-potential [93, 117–119]. Moreover, zeta-potential measurement can also be applied to determine the dispersion effect of SWNTs; usually, when the absolute value of zeta-potential $|\zeta| > 15$ mV, the CNT is well dispersed in solvents and expected to be stable. Dispersion quality metrics can also be significantly improved by using surfactants coated on nanotubes to give hybrids with zeta-potential of 100 mV or higher [120].

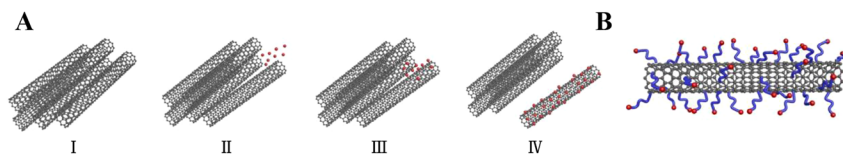


Figure 1: Dispersion of CNTs with surfactants.

(A) Mechanism of SWNT isolation from bundles by ultrasonication and surfactants. Kim et al. [114]. © The Royal Society of Chemistry 2020.

(B) Random adsorption of surfactant molecules on a single SWNT. CNT, carbon nanotube; SWNT, single-walled CNT. Yurekli et al. [116].

© American Chemical Society 2004.

2.2.2 Amide solvents

The π bonding of graphene surface and large molecular weight of CNTs render pristine CNTs insoluble in common aqueous and organic solvents. In addition, the high curvature of the small tubular geometry makes the surface increasingly electrophilic, and an external dispersant is necessary to incorporate into the medium for dispersing SWNTs. Some amide solvents are demonstrated to be able to directly separate SWNTs, such as N-methyl-2-pyrrolidone (NMP), dimethylformamide (DMF), dimethylacetamide, dimethyl sulfoxide, N-methylformamide, hexamethylphosphoramide [121–126], etc. In all solvents described previously, NMP is experimentally proved to be unique. Dispersion theory also verified that for the ideal solution in which SWNTs are thermodynamically soluble by amine e-pair donation and stabilized by steric hindrance, the free energy of mixing ΔG_{Mix} should be negative.

$$\Delta G_{\text{Mix}} = \Delta H_{\text{Mix}} - T\Delta S_{\text{Mix}}$$

where ΔH_{Mix} and ΔS_{Mix} are the enthalpy and entropy of mixing, respectively, which are related to several solvent and SWNT parameters. When the solvent surface energy flux matches approximately 70 mJ/m^2 of nanotube/graphite surface, as well as solvent surface tension reaches closely to 40 mJ/m^2 , such solvent can effectively disperse SWNTs and NMP meets these parameters [127].

However, SWNTs dispersed in NMP solution is generally limited by 0.02 mg/mL , which is just below the transition point from dilute to semidilute regime of filaments of CNT dimensions [121]. The van der Waals attraction between nanotubes in close state is still strongly attracted. Therefore, a stable solution can only be achieved in low-concentration dispersion to increase the interaction distance, and these limitations may influence desired performance for SA application, that is, modulation depth.

Polyvinylpyrrolidone has been verified to perform as perfect assistance to increase loading and stability of SWNTs in NMP [124, 128, 129].

2.3 Characteristics of CNT SAs

Various methods have been used to characterize the dispersion effect and nonlinear optical properties of SWNTs. For example, UV–Vis-IR optical absorption spectroscopy is a powerful tool to determine the structure of CNTs and study the influence of ultrasonication process. Power-dependent characterization can be implemented by Z-scan (open and closed aperture) which can be applied to measure the nonlinear optical characteristics (saturable absorption and optical limiting). Photoluminescence spectroscopy can be used to identify different species of SWNTs in the sample and is also widely used to monitor the quality of dispersion, SWNTs bundling and enrichment of specific chirality. Pump probe spectroscopy is commonly utilized to measure the recovery time as well as excitation relaxation time. Raman spectroscopy on SWNTs is widely adopted to confirm the presence and diameter distribution of SWNTs. Detailed description about these techniques has been reviewed elsewhere [68, 77, 78, 124, 129–147].

Another popular type of power-dependent transmission measurement is depicted in Figure 2A and the typical results are shown in Figure 2B. The fitted curve can be expressed as

$$T(I) = 1 - \alpha(I) = 1 - \frac{\alpha_0}{1 + I/I_{\text{sat}}} - \alpha_{\text{ns}}$$

Where I is input light intensity, I_{sat} is saturation intensity (the intensity necessary to reduce modulation depth to half of initial value), α_0 is modulation depth and α_{ns} is nonsaturable absorption loss.

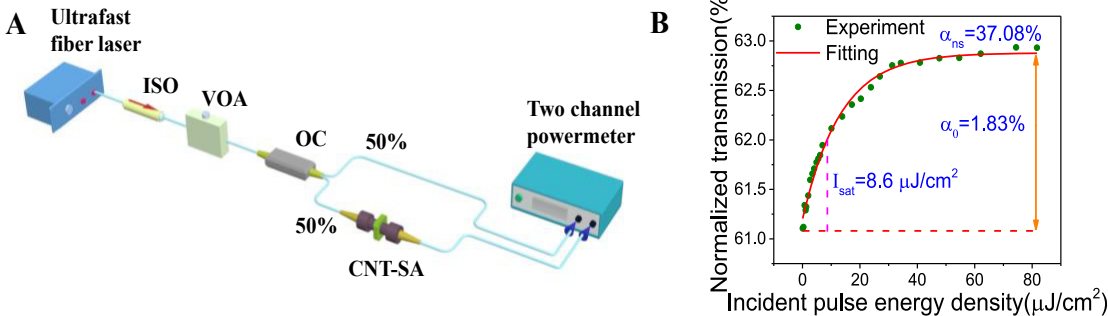


Figure 2: Power-dependent transmission measurement.

(A) Experiment setup. ISO, isolator; VOA, variable optical attenuator; OC, output coupler. (B) Measured results from CNT–polyvinyl alcohol (PVA) film.

These parameters play essential roles in output characteristics of ultrafast fiber laser system. I_{sat} keeps relationship with the mean slope of the normalized transmission curve, which is related to the amount of resonance absorption tubes at a specific wavelength, suitable selection of types and diameter distribution of SWNTs can decrease the threshold of mode locking. The threshold is also related to the nonsaturable absorption loss, mainly arising from polymer matrix, amorphous impurities, residual metal catalyst. And unevenness and rough surface of SWNTs polymer composites may lead to large elastic scattering meanwhile increase nonsaturation absorption loss. This may weaken the performance of lasers, such as higher threshold of mode locking, poorer signal-to-noise ratio and lower output power. Modulation depth is related with intrinsic photobleaching effect of SWNTs. Higher modulation depth can result in shorter pulse width and can be obtained from higher SWNT loading and thicker sample. Nevertheless, the increase in nonsaturable absorption loss may exist. The ratio of modulation depth to nonsaturable absorption loss can be used to describe performances of SWNT SAs, and literature reported that this ratio was usually less than 1, much smaller than commercial SESAM SAs, which may hinder their commercial development. Thus, the fabrication of SWNT polymer composite SAs suitable for different fiber laser applications still requires massive experiment data to continuously optimize and control several parameters.

Despite such performances of SAs, uniformity and stability of samples decide the reproducibility and commercial possibilities. Some study revealed that the absorption mapping can be helpful to determine uniformity [74]. Besides, the thickness distribution and surface roughness of film-type CNT SAs is also an essential factor affecting the final performances. Long-term stability against environment and operation states also dominates in the sample preparation, especially for water-soluble polymer and high-power operation condition; these can be demonstrated by absorption spectroscopy, modulation depth measurement and Raman spectroscopy [148].

Raman mapping is an effective characterization method for purity assessment and chirality assignment [149–152]. Raman mapping for purity of CNT-PVA film with a scanned step of $10\ \mu\text{m}$ within an area of $250 \times 250\ \mu\text{m}$ under the excitation of $532\ \text{nm}$ is shown in Figure 3A. Figure 3B and C shows raw spectra for each pixel in Figure 3A. Actually, it is hard to distinguish distribution of *m*-SWNTs and *s*-SWNTs because CNTs in this sample are bundled, leading to overlapped peak in Raman spectra. However, we can also obtain the homogeneity, defects, diameter distribution information from Raman mapping. Figure 3B displays integrated intensity of *G*-peak mapping. It is obvious that intensity in the left is higher than that of right rather than uniform distribution. It can be caused by uneven surface or inhomogeneity of bundled CNTs. In Figure 3C, we can also observe that the value of $I(D)/I(G)$ is from 0.12 to 0.16 which is very low and the tendency is similar to Figure 3B. Therefore, there is not much disorder and defects in the measured sample. These measured Raman mapping results are beneficial to preparation of CNT films and characterization. Generally speaking, information of conductivity and chirality distribution can be further obtained by using tip-enhanced Raman scattering technique [153–155]. If CNTs in the film are almost individual rather than bundled, mapping results must be a more accurate and easier reference to distinguish the distribution of various CNTs.

2.4 Development of CNT SAs

Since the first demonstration of SWNTs applied as an SA in a mode-locked fiber laser system, SWNT SAs have been utilized by different research groups based on various techniques and operation types, meanwhile maintaining all-fiber configuration. For instance, the most popular type of SWNT SA used in fiber lasers concentrates on polymer composite film, which is sandwiched between fiber connectors, including host matrix such as polyvinyl alcohol (PVA) [156, 157], poly(ethylene oxide) [158], polystyrene



Figure 3: Raman mapping results.

(A) Scanned area of Raman mapping under the excitation of $532\ \text{nm}$ with a step of $10\ \mu\text{m}$. (B) Integrated intensities map for *G*-band. (C) Integrated intensities map for *D*-band/*G*-band.

[159], polyimide (PI) [160–162], poly(methyl methacrylate) [163, 164], carboxymethyl cellulose [165, 166], polycarbonates (PC) [167, 168], etc. Another kind of SWNT SA attached to the optical fiber end comes from optical deposition in which SWNTs are usually dispersed in DMF or ethanol solution [169, 170]. Such interaction types originate from direct interaction between CNT and transmission light; however, high-power tolerance may be a limit. Other approach based on evanescent field can be a candidate and SWNTs can be coated on a D-shaped fiber [171, 172], microfiber [173, 174], or injected into microslot [175, 176], photonic crystal fiber [177] and hollow core fiber [178]. Recently, the development of SWNT SAs pays more attention on power handling, environmental stability and more outstanding SA characteristics including sol–gel method and glass doping [179, 180].

3 Fiber lasers based on CNT SAs

3.1 G-Hz fiber lasers

Nowadays, mode-locked fiber laser operating at a few gigahertz repetition frequencies has been a red-hot direction of research owing to the potential applications such as optical sampling [181], optical communication [182] and optical frequency metrology [183]. Exploiting a short cavity and passively harmonic mode locking (PHML) are cost-effective choices while maintaining short pulse width at the same time [184, 185].

CNTs prefer to be implemented in high repetition rate fiber laser offering attractive advantages including ultra-fast recovery time, excellent fiber compatibility, wide operation wavelength range, ease of fabrication, miniature size, low loss, etc. [186]. Specifically, CNTs are applicable to different waveband provided that the tube diameter distribution is well controlled [187]. In consequence, it is feasible to realize high repetition rate pulses in different waveband (e.g., 1 μm , 1.5 and 2 μm) using CNT SAs.

Passively mode-locked fiber laser with fundamental repetition rate operation is characterized by simple construction and high output stability and offers incentives for producing shorter pulse duration, where the pulse frequency is negatively related to the cavity length [188]. Normally, such type of laser operates at a few tens of megahertz because of the cavity length of few meters. To push pulse frequency up to few gigahertz in the fundamental mode-locking regime, as short as a few centimeters cavity length should be guaranteed. Fortunately, CNTs possess inherent merits of excellent fiber compatibility, minor dimension, small loss as well as the applicability to

work in both transmission mode and reflection mode, which is the key enabler for mode locking in a short cavity.

Some attempts to realize high repetition rate fiber laser in ring cavity configuration with CNT SAs have been made in the last decade. Nicholson et al. have shown a 447 MHz fiber laser with 270 fs pulse duration using a multifunctional integrated device, which is the highest fundamental frequency ring fiber laser with CNT SAs to date [189]. In 2015, to damp environmental turbulence, an all-polarization-maintaining fiber laser with 358.6 MHz was demonstrated. The generated pulse duration ranged from 240 to 550 fs and the degree of polarization (DOP) was 98.7% [190]. Despite the fact that the ring configuration is conducive to be dispersion managed leading to substantial reduction of pulse width, it is hard to diminish the cavity length further to achieve gigahertz pulses.

Instead, Fabry–Pérot laser (FFPL) in virtue of more compactness eliminates such restriction and exhibits a few centimeters cavity length easily, resulting in gigahertz pulse generation. 5 GHz FFPL with only a 2-cm cavity length based on a CNT SA by Yamashita et al. was realized as early as 2005 [184]. The typical FFPL configuration is schematically presented in Figure 4 [191]. The laser configured with two high reflective (99%) mirror-coated ferrules and 2 cm highly co-doped Er:Yb fiber to provide sufficient gain. The CNTs sprayed on the right high reflective mirror form a thin film exhibiting distinct advantages of reasonable modulation depth, low insertion loss and extremely miniaturized size, which is favorable in an extremely short cavity. The laser shows high finesse benefiting from the two high reflective mirrors as well as the low loss CNT SAs. Two years later, the same group reduced the cavity length further into 9 mm by using a mirror-coated semiconductor optical amplifier as gain medium. As a result, the pulse frequency extended to 17.2 GHz [186]. In 2011, the FFPL cavity was maximally miniaturized via a further optimization of gain fiber where only a 5-mm phosphosilicate fiber heavily codoped with erbium and ytterbium was incorporated. The generated pulse frequency attained 19.45 GHz, which is the highest fundamental frequency yet reported for CNTs mode-locked fiber laser [191]. In addition, they obtained stable supercontinuum using this type of laser operating at 9.63 GHz as a seed source.

Nevertheless, the FFPL requires the special high-gain fiber and extremely minimal fiber devices, which needs sophisticated production and high cost, making it cumbersome to manipulate and difficult to utilized intensively in practical applications, while the further expansion of fundamental repetition rate in the ring cavity scheme is unattainable because of more stringent

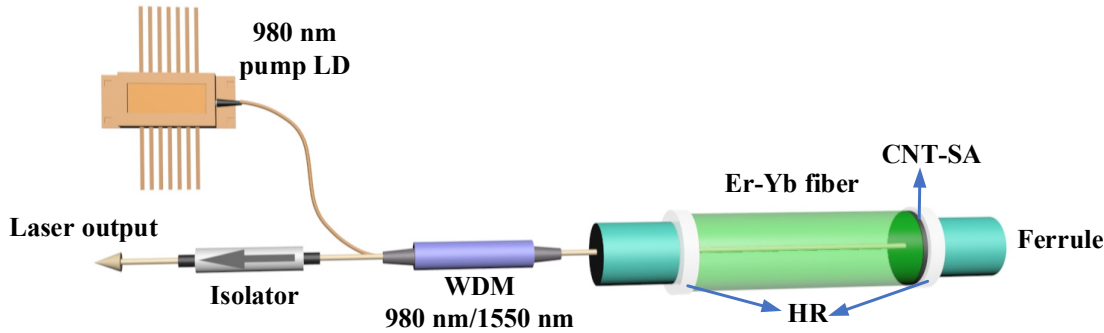


Figure 4: FFPL mode-locked by CNT SAs. WDM, wavelength division multiplexing; HR, high reflector; CNT SA, carbon nanotube saturable absorber. Martinez et al. [191]. © Optical Society of America 2011.

requirement of cavity length. Furthermore, the short cavity can be hard to be mode-locked unless the cavity with high finesse incorporates high-gain fiber and high-quality SAs featuring low loss and miniature size [184, 186, 191]. PHML is a special phenomenon where several uniform pulses circulate in cavity because of high pump power with equal distribution indicating the occurrence of frequency multiplication [192]. Fortunately, PHML revealed as a critical pathway to overcome these constraints opens up the possibility of achieving high repetition rate and maintaining simple laser configuration without reducing cavity length and extra modulator at the same time [193].

The first demonstration of gigahertz CNT-based PHML fiber laser is mode-locked by evanescent-type CNT SAs, which is illustrated in Figure 5A [194]. The spin-coating process is introduced to deposit a CNT layer onto a side-polished fiber, rendering longer interaction length between light and CNTs [195]. Benefitting from that, the evanescent-type CNT SA simultaneously offers mechanical robustness and high damage threshold, which is proved to be useful for high repetition rate pulse generation. Likewise, the evanescent-type CNT SA also can be formed by depositing CNTs onto microfiber [196, 197] or *D*-shaped fiber [172]. The developed laser permits the generation of 913.16 MHz pulses at the 34th harmonic with good noise characteristics. In 2012, this group engineered the single pulse energy by optimizing the average cavity dispersion and optical spectral bandwidth for the purpose of more intensive pulse splitting. Supported by the soliton area theorem, through dispersion engineering and nonlinearity mapping, they finally extended pulse frequency to 5 GHz with 40 dB side mode suppression ratio (SMSR) under 400 mW pump power. This is the highest repetition rate pulse to be achieved in PHML fiber laser with CNT SAs [198].

However, the significant weakness of this type of CNT SA should be pointed out that the structure of specialty fiber device makes a strong impression on the performance

of CNT SAs, inevitably introducing complexity to the cavity design. By contrast, film-type CNT SAs mitigate such weakness and offers high adaptability, good reliability combined with excellent portability because it can be easily integrated into laser by embedding it into two fiber connectors, as shown in Figure 5B. But the direct interaction has inherent shortcoming of low damage threshold, challenging the generation of GHz pulses in PHML fiber laser where relatively high pump power is normally required [199, 200].

Enlightened by the investigation of Jun et al. [198], a reduction of pulse energy should be carried out and thereby high-order HML, to some extent, represented high repetition rate, can be realized under relatively low pump power. By using this method, we obtained 42nd HML pulses at repetition frequency up to 1.15 GHz from film-type CNT SA-based fiber laser under pump power of 321 mW [201]. Taking advantage of wide operation wavelength range of CNTs, *L*-band PHML fiber laser using CNT film was proposed first in the same year [202]. We have carried out a systematic exploration on the effects of average cavity dispersion and spectral bandwidth on HML in *L*-band using similar laser scheme [203]. It was found that the single pulse energy was eventually determined by the product of the average cavity dispersion and spectral bandwidth (dispersion bandwidth product, DBP) if other parameters such as average nonlinearity parameter, the time bandwidth product and center wavelength were similar. The effective optimization of DBP resulted in a considerable reduction of pulse energy, subsequently generating 2.04 GHz repetition rate pulses under 205 mW pump power. The obtained pulse energy was as low as 3.44 pJ and the pulses showing good stability evidenced by SMSR value of 36.5 dB. Later, a PHML fiber laser with further frequency extension (2.4 GHz), shorter pulse duration (863 fs), better stability (40 dB), and higher pump power efficiency (17 MHz/mW) was demonstrated where a

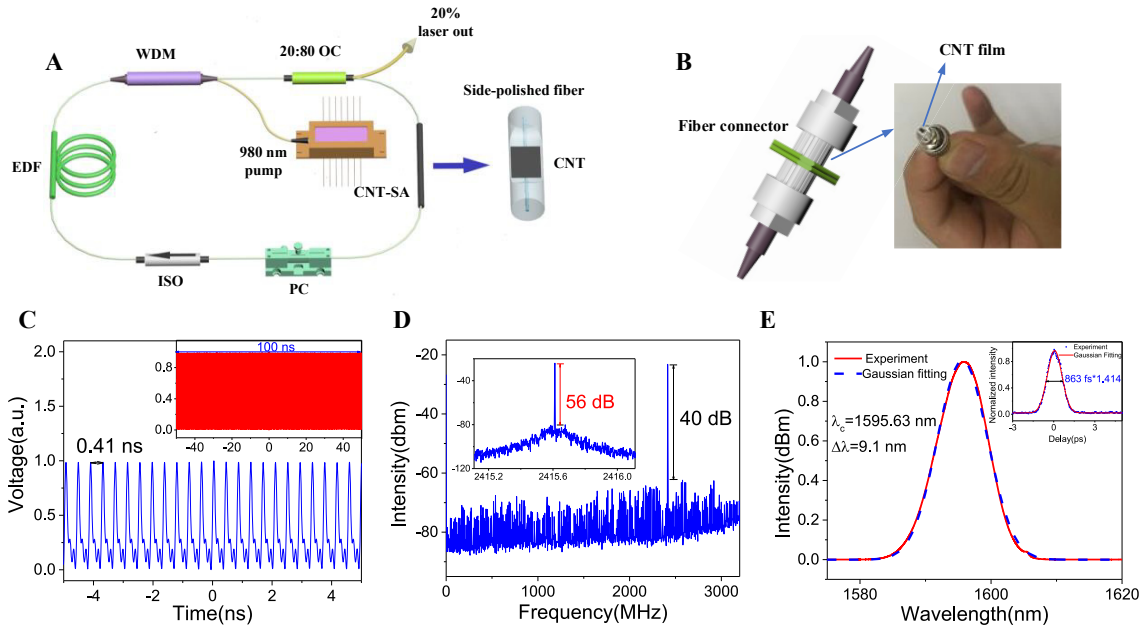


Figure 5: (A) PHML fiber laser with CNTs deposited on side-polished fiber. EDF, Er-doped fiber; ISO, isolator; PC, polarization controller; OC, output coupler. Jun et al. [194]. © Optical Society of America 2011. (B) Structure of a film-type CNT SA. (C) The oscilloscope trace with a repetition rate of 2.415 GHz. Inset: the pulse train spanning 100 ns. (D) The RF spectra (span: 3.2 GHz, resolution: 10 kHz). Inset: RF spectra (span 1 MHz, resolution: 1 kHz). (E) The corresponding optical spectrum in linear scale. Inset: autocorrelation trace fitted by Gaussian profile. Huang et al. [204]. © IEEE 2020.

CNT film with lower modulation depth was incorporated [204]. The pulse performances were shown in Figure 5C–E, and the corresponding pulse energy was decreased to 2.41 pJ, which is the lowest pulse energy ever obtained in a PHML fiber laser using a CNT SA, indicating effective cavity management. Recently, a 902 MHz vector soliton fiber laser corresponding to 51st harmonic from a similar cavity stimulated by torsional-radial TR_{2m} acoustic modes was responsible for pulse stabilization [205]. If the tube diameter distribution is well controlled, CNTs can extend the accessible working wavelength toward 2 μm . However, attempts to realize HML fiber laser in mid-infrared such as 2 μm using CNT SAs is very scarce. So far, Harun et al. have demonstrated the generation of 25th HML at 1901.6 nm corresponding to repetition rate of 214 MHz [206]. It is anticipated that GHz pulses can be achieved from CNT-based PHML 2 μm fiber laser under effective management of single pulse energy as well as the improvement of CNT SAs performance.

3.2 Bidirectional mode-locked fiber lasers

In general, conventional ultrafast fiber lasers introduce an optical isolator to suppress the stray reflected light in the

cavity to reduce the mode-locking threshold, so the mode-locked fiber laser usually operates in a unidirectional state. By comparison, bidirectional ultrafast fiber lasers capable of generating pulses in both clockwise (CW) and counterclockwise (CCW) directions show great potential in optical sensing [39, 207], dual-comb spectroscopy [208] and terahertz spectroscopy [209]. Since the first all-fiber bidirectional passively mode-locked ring laser was reported by Kieu and Mansuripur in 2008 [210], this kind of bidirectional all-fiber ultrafast laser has attracted extensive attention in recent years. Whether the output characteristics in the two directions of the laser maintain high consistency or difference, providing two distinct design concepts for the bidirectional mode-locked fiber laser. Originally, researchers concentrated on obtaining the bidirectional ultrashort pulses with similar performance by ensuring the symmetry of the laser cavity as much as possible [211]. Afterward, the all-fiber mode-locked laser with the ability to generate bidirectional output with distinct properties in terms of repetition rate, spectrum shape, central wavelength, pulse duration in one same laser can meet various application requirements and exhibits broader prospects [212].

Owing to the colliding pulse mode-locking mechanism and superior optical properties of CNTs as an SA, the self-starting mode-locking operation in both CW and CCW

directions can be simultaneously achieved in the all-fiber laser. In Ref [210], the first bidirectional passively mode-locked all-fiber laser choose a short fiber taper embedded in a CNTs/polymer composite as an SA to achieve bidirectional mode locking simultaneously with bidirectional pumping as shown in Figure 6A. The generated two femtosecond pulses exhibited the same central wavelength. Liu et al. proposed a bidirectional fiber soliton laser using an SWNT/PVA mode-locker as shown in Figure 6B and the asymmetry cavity and fiber birefringence lead to different central wavelengths, pulse durations and repetition rates [213]. They also found that the nonequal repetition rates of two pulses are attributed to the nonidentical operating wavelengths. Unlike the previous bidirectional soliton output, a bidirectional Er-doped fiber laser based on the mixture of graphene and SWNTs was also demonstrated [214]. As shown in Figure 6C, the laser can deliver two different types of pulses (conventional soliton and dissipative soliton) in opposite directions by adjusting the two attenuators to precise control the intracavity loss in each direction. This kind of all-fiber switchable conventional soliton and dissipative soliton mode locking is very convenient for practical applications. Unfortunately, it cannot achieve mode-locking operation in both directions simultaneously. Then in quick succession, a bidirectional stretched pulse in a SWNT-based Er-doped fiber laser was experimentally demonstrated [215], as well as bidirectional bound solitons were also achieved in an ultracompact linear cavity mode-locked by CNTs polymer film [216]. Apart from different kinds of pulse-shaping mechanisms, the pulses in CW and CCW directions with other different features such as wavelength characteristics and repetition rates have been investigated. By employing a polarization-dependent four-port circulator, Liu et al. developed an operation-switchable bidirectional mode-locked fiber laser with a CNT-based SA (Figure 6D) [217]. The pulse widths in both directions were 600 and 480 fs, respectively. The corresponding fundamental repetition rates were 12.48 and 16.46 MHz, respectively. In 2014, a dual-wavelength bidirectional femtosecond *L*-band fiber laser incorporating an SWNT SA was realized in Ref [218] as a result of the gain difference between counterpropagating directions. In addition, Krylov et al. [219] investigated the generation regimes of bidirectional Er-doped fiber laser with a combination of SWNT-based SA and nonlinear polarization evolution as shown in Figure 6E, which can achieve fine control over pulse characteristics for both CW and CCW directions through the appropriate intracavity loss control. Meanwhile, Chernysheva et al. utilized the similar isolator-free hybrid mode-locked fiber laser operating in both unidirectional and bidirectional regimes via the precise

control of intracavity birefringence and state of polarization [220]. More recently, with the increasing interests of 2 μm eye-safe wavelength region, Jiang et al. [221], Kieu et al. [222] and Li et al. [223] demonstrated all-fiber bidirectional mode-locked ring lasers operated at 2 μm using a CNT SA successively. It is noteworthy that the bidirectional mode-locked Er-doped fiber laser and thulium-doped fiber laser shown in Figure 6F and G with tunable frequency difference have already used as single-cavity free-running dual-comb sources [208, 222].

3.3 Vectorial mode fiber lasers

As a special class of optical beams, the mode-locked cylindrical vector beams (CVBs) have attracted considerable attention in a wide variety of potential applications, including laser material processing [224], optical trapping [225] and particle manipulation [226]. Unlike the traditional Gaussian beam with uniform polarization distribution, the CVBs have cylindrical symmetry in polarization and a donut shape intensity distribution and can be divided into radial, azimuthal and hybrid polarization beams. Since the 1970s, various kinds of methods for generating CVBs have been reported in succession, which are classified as passive or active depending on whether a gain media is used. The passive approaches utilize the extra-cavity spatial polarization-selective device to convert the incident spatially homogeneous polarization beams into spatially inhomogeneous polarization beams [227, 228]. And the active approaches usually introduce a birefringence crystal or a dichroic crystal into the laser cavity to suppress the oscillation of the fundamental mode beams and make the CVB modes resonate [229–231].

However, the free space devices utilized in above methods add additional insertion loss and assembly complexity to fiber-based laser, communication and sensing systems. Consequently, the all-fiber laser CVB source has received increasing interest in the last two decades because of its compact structure, excellent flexibility and high efficiency. For the few-mode step-index optical fiber, the radially and azimuthally polarized beams correspond to the eigenmodes TM₀₁ and TE₀₁, respectively [232]. Therefore, it is an ideal solution to generate CVBs using few-mode fiber (FMF)-based components with transverse-mode selection. To date, different ways to excite high-order modes in optical fibers have been developed including the use of offset splicing spots (OSSs), fiber gratings and mode selective couplers (MSCs). Zheng et al. proposed an all-fiber continuous-wave Yb-doped laser to generate CVBs by introducing misalignment of two fiber-

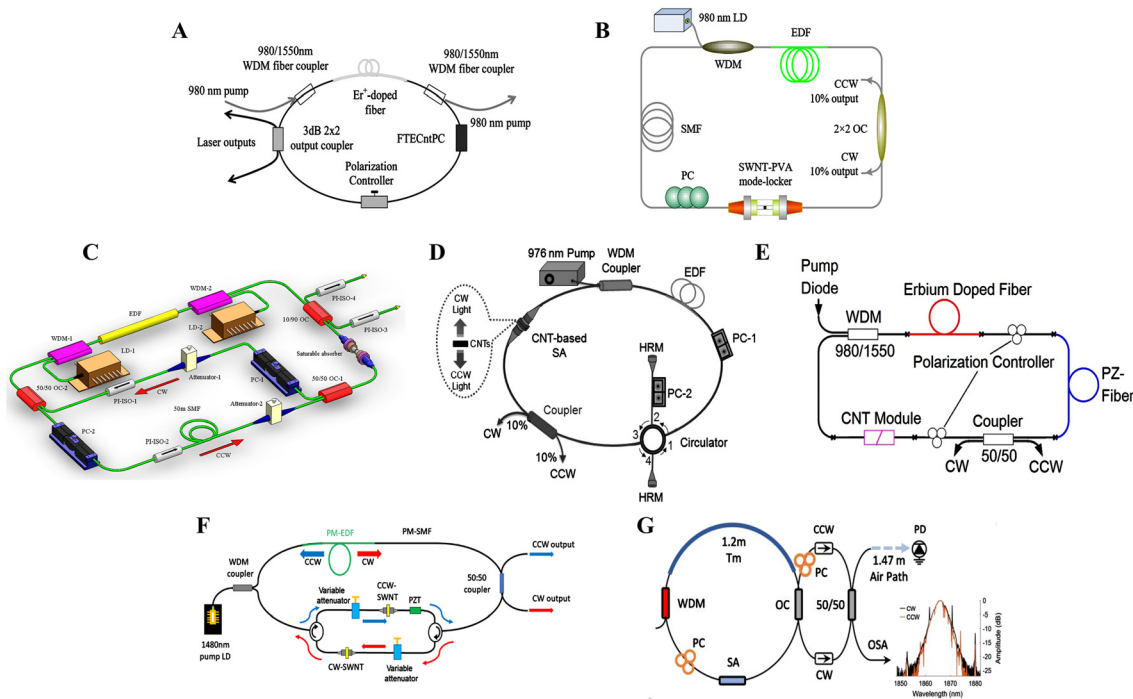


Figure 6: Typical schematic diagrams of the bidirectional fiber laser mode-locked by CNT SAs.

(A) The first bidirectional mode-locked all-fiber laser with bidirectional pumping. Kieu et al. [210]. © Optical Society of America 2007. (B) A bidirectional soliton laser can obtain two stable solitons simultaneously with the same or different central wavelength. Zeng et al. [213]. © Optical Society of America 2013. (C) A bidirectional mode-locked fiber laser based on a mixture of graphene and SWNTs generating dissipative soliton and conventional soliton in opposite directions with intracavity attenuators. Cui et al. [214]. © Optical Society of America 2013. (D) An operation-switchable bidirectional mode-locked fiber laser using a four-port circulator. Liu et al. [217]. © IEEE 2014. (E) A bidirectional hybrid mode-locked fiber laser with a combination of SWNT SA and NPE. Krylov et al. [219]. © Optical Society of America 2016. (F) A bidirectional Er-doped dual-comb fiber laser. Saito et al. [208]. © Optical Society of America 2019. (G) A bidirectional thulium-doped dual-comb fiber laser. Olson et al. [222]. © IEEE 2018. SWNT, single-walled carbon nanotube; CNT SA, carbon nanotube saturable absorber; NPE, nonlinear polarization evolution.

based collimators in 2010 [233]. Then, Sun et al. improved the output mode and polarization purity to higher than 94% in a single-wavelength CVB fiber laser with a few-mode fiber Bragg grating (FBG) [234]. Furthermore, the pulsed CVB fiber lasers using Q -switching or mode-locking technique have been reported in recent years with the growing demand for high energy and narrow pulse. In 2015, an all-fiber mode-locked Yb-doped radially polarized laser by incorporating two cascade FBGs with the figure-8 cavity was experimentally demonstrated [235]. Yan et al. achieved a Q -switched fiber laser with CVB output modes using Bi_2Te_3 as SA and a few-mode FBG as a polarization-selective output coupler [236]. Meanwhile, an actively mode-locked all-fiber CVB laser using a four-mode FBG for transverse mode selection was demonstrated in 2016 [237]. Soon afterward, Wan et al. fabricated an MSC with high mode conversion efficiency by weakly fusing technique and incorporated it into the figure-8 cavity to realize a passively mode-locked CVB fiber laser with high efficiency and high mode purity [238].

As for the mode-locking method for producing ultra-short pulsed CVBs, CNTs have become one of the promising SAs. For the past few years, CNT mode-locked CVB fiber lasers have emerged in the research field. In 2016, Zhou et al. reported a self-starting mode-locked all-fiber laser based on CNT that generated radially polarized beam (RPB) emission with an OSS and a few-mode FBG [239]. As shown in Figure 7A, they obtained an RPB with high mode purity of 98.03% by adjusting the polarization controllers. Mao et al. and Cai et al. successively utilized a similar method to achieve ultrafast CVB fiber lasers mode-locked by CNT SA as shown in Figure 7B and C [240, 241]. The output polarization status is switchable between radially and azimuthally polarized states by adjusting the polarization controllers while the mode-locking state can always be maintained. To overcome the large loss caused by OSSs and the narrow bandwidth for mode conversion of the FBG to limit the output performance of CVB lasers, the all-fiber MSC composed of single mode fiber (SMF) and FMF was proposed to improve the slope efficiency and operating

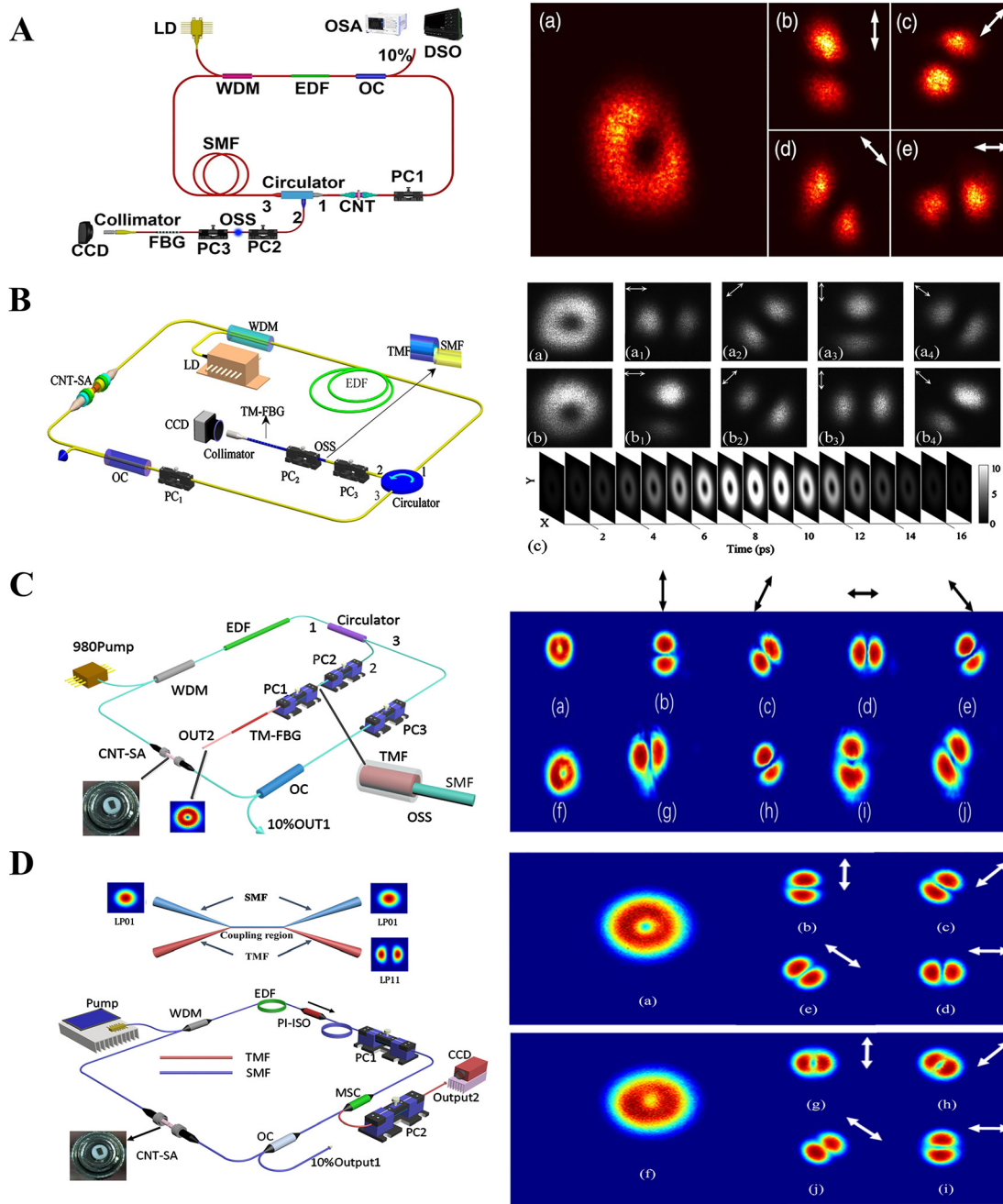


Figure 7: Typical experimental setup and intensity distributions of the mode-locked fiber laser with CVB generation based on CNT SAs. (A–C) The mode-locked CVB all-fiber lasers with an OSS and a few-mode FBG. Zhou et al. [239]. © Chinese Laser Press 2016; Mao et al. [240]. © AIP Publishing 2017; Cai et al. [241]. © MDPI 2018. (D) The mode-locked CVB all-fiber laser with a home-made mode selective coupler composed of SMF and FMF. Zhang et al. [243]. © IEEE 2018. CNT SA, carbon nanotube saturable absorber; CVB, cylindrical vector beam; OSS, offset splicing spot; FBG, fiber Bragg grating; SMF, single mode fiber; FMF, few-mode fiber.

wavelength of fiber lasers with CVB emission [242]. In 2018, a switchable dual-wavelength femtosecond CVB fiber laser based on CNT for mode locking and MSC shown in Figure 7D for broadband mode conversion was demonstrated by Zhang et al. [243]. In addition to being able to

obtain both radially and azimuthally polarized beams, the CVB laser also can operate and switch at 1532.5 and 1555.5 nm through tuning the intracavity polarization controller due to the birefringence filtering effect introduced by the MSC.

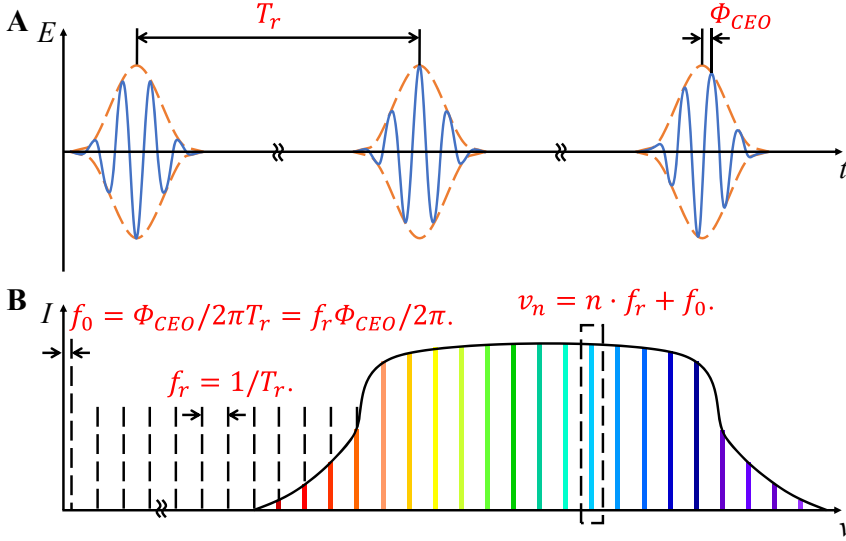


Figure 8: A optical frequency comb based on femtosecond mode-locked laser in the (A) temporal, and (B) frequency domain. Kim et al. [250]. © Optical Society of America 2016.

3.4 Comb

Since the realization of the first fully stabilized self-referenced optical frequency comb (OFC) with a Ti:sapphire mode-locked laser in 2000 [244], it has revolutionized optical frequency metrology and precision spectroscopy with its superior stability and accuracy. In addition, as the OFC has evolved from a complex and sensitive laboratory device to a robust and compact system in recent years, it has also been used as a reliable and instrument in many other scientific research fields, such as optical atomic clocks [245], ultra-low-noise microwave signal generation [246], precision frequency/time transfer [247], absolute distance measurements [248] and arbitrary optical waveform generation for optical communication [249]. In particular, the mode-locked fiber laser frequency comb has achieved the greatest commercial success and become the most widely used OFC system because of its compact structure, robustness, ease of operation and high energy efficiency.

In simple terms, an OFC is essentially a phase-stabilized mode-locked laser capable of generating a set of equidistant spectral lines. As shown in Figure 8A [250], the optical output of a mode-locked laser in time domain is a periodic train of ultrashort pulses with pulse-to-pulse period, T_r . In the frequency domain as shown in Figure 8B, this pulse train can be expressed as a Fourier series of equidistant optical frequencies with mode spacing corresponding to the repetition rate, $f_r = 1/T_r$. Owing to the dispersive effects in the laser cavity, the carrier oscillation and the pulse envelope propagate with different phase and

group velocities, respectively, leading to a phase shift between the carrier phase and pulse envelope, which is called the carrier-envelope offset phase (Φ_{CEO}). Therefore, the carrier-envelope offset frequency f_0 is expressed as $f_0 = \Phi_{CEO}/2\pi T_r = f_r \Phi_{CEO}/2\pi$. As a result, the optical frequency of n th comb mode (ν_n) can be determined by f_r and f_0 , such that $\nu_n = n \cdot f_r + f_0$. This equation is referred to as the comb equation. If the two degrees of freedom, f_r and f_0 , can be detected and stabilized, any other longitudinal mode frequency within the spectral range of the mode-locked laser can be accurately determined, thereby realizing precise optical frequency measurement.

For a femtosecond mode-locked fiber laser, the repetition rate f_r is generally in the order of MHz, which is in the microwave frequency range and can be directly accessed by detecting the amplitude modulation of the pulse train utilizing a conventional photodetector. However, f_0 is related to the carrier frequency which is in the order of THz and difficult to access directly. By adopting the f -to- $2f$ self-referencing method [251], the low-frequency component (ν_n) of the octave supercontinuum is frequency doubled and is superimposed with the corresponding high-frequency component (ν_{2n}), so the obtained beat note frequency, $2 \cdot \nu_n - \nu_{2n} = 2 \cdot (n f_r + f_0) - (2n \cdot f_r + f_0)$, is the carrier-envelope offset frequency f_0 . For stabilization, f_r is typically controlled by tuning the laser cavity length with a wide bandwidth piezoelectric transducer or an electro-optic phase modulator. For the case of f_0 , it is generally stabilized by active modulating the pump power and the intracavity loss or achieved “offset-free” comb [252] by passive eliminating the f_0 via difference frequency generation.

As the key source of fiber-based OFC systems, the mode-locked fiber laser is expected to generate ultrashort pulses with high power, high repetition rate, low phase noise and low timing jitter. The SWNT, as one of the effective SA for ultrafast fiber laser, is considered to be a promising candidate in all-fiber frequency comb systems. It is capable of realizing self-starting mode locking in an all-polarization-maintaining cavity and obtaining stable ultrashort pulse with high repetition rate in a more compact and robust design. Compared with the conventional SESAM SA, SWNT SA exhibits a shorter relaxation time constant and is therefore more conducive to the generation of femtosecond pulses.

Back to 2009, Lim et al. demonstrated a phase-stabilized 167 MHz mode-locked Er-doped fiber laser frequency comb based on a CNT SA for the first time [253]. The CNT deposited on the end of an FC/APC connector into the cavity which allowed for the all-fiber configuration is shown in Figure 9A. The integrated phase noise of f_0 error signal was 0.35 radians from 100 to 107 Hz which is comparable with 0.48 radians of the phase-stabilized frequency comb mode-locked by NALM. Subsequently, an all-fiber frequency comb utilizing a tapered-fiber CNT with free-running f_0 linewidth of ~ 20 kHz in Figure 9B was reported by Kieu et al. in 2011 [254]. The integrated phase noise of f_0 was ~ 0.8 radians from 10 to 400 kHz. Afterward, Kieu et al. have successively proposed an efficient mid-infrared frequency comb for wavelengths longer than $6 \mu\text{m}$ [255], a real-time Er-doped fiber laser free-running dual-comb source [256], an octave-spanning free-running dual-comb source [257], a robust all-in-fiber polarization-maintaining frequency comb oscillator [258], a thulium-doped fiber laser free-running dual-comb source [222]. The above systems were all mode locking by fiber taper embedded in a CNT/polymer composite. In the meantime, Nishizawa's group used the SWNT PI film to achieve soliton [259] and stretched pulse [260] mode locking in Er-doped fiber lasers and accomplish the stabilization of f_r and f_0 adopting similar configurations depicted in Figure 9C and D. Later on, they also have successively used the SWNT PI film-based Er-doped mode-locked fiber laser to develop the offset-free mid-infrared OFC system at $3 \mu\text{m}$ region [261], all-polarization-maintaining fiber frequency comb [262], octave-spanning coherent supercontinuum comb [263], wavelength-tunable narrow linewidth OFC source [264], all-polarization-maintaining bidirectional dual-comb fiber laser [208]. In addition, a lot of efforts have been made in dual-comb fiber laser with SWNT SAs by Zheng et al. since 2012 [265]. In the last few years, driven by the increasing attractiveness of low-complexity multicombs in the field of spectroscopy, frequency and distance measurement, they have reported dual-comb, tricomb and even quad-comb generation from a simple

single-cavity mode-locked fiber laser with an SWNT SA by leveraging simultaneous multiplexing in wavelength and polarization [266, 267]. Based on the rapid development of fiber frequency comb technology, we believe that the all-fiber frequency comb system using an SWNT SA brings a broad prospect as a robust, portable, cost-effective and high-performance fiber frequency comb.

3.5 Mode-locking dynamics

Ultrafast fiber laser, referred to as a typical dissipative system, is an ideal platform for studying nonlinear dynamics. However, the complex mode-locking dynamics are directly involved with environmental disturbance, intracavity polarization state, laser system design, most importantly, the applied mode locker. In addition, the ability of self-starting is quite crucial, especially in the investigation of soliton booting dynamics. Given that CNTs with great performance are used as a mode locker, the self-starting operation can be realized easily and the influence of polarization state and environmental disturbance can be mitigated due to the CNTs' feature of polarization insensitivity. Therefore, CNT-based fiber laser is an excellent platform to research various kinds of soliton dynamics.

Soliton generation dynamics in fiber laser have been a red-hot object long before [268]. However, most studies concentrated on stimulation instead of experiment owing to the limitation of conventional measurement apparatuses. Fortunately, dispersive Fourier transformation (DFT) technique opens a portal to record the real-time spectral evolution of the soliton buildup process [269–272]. For a more comprehensive review in DFT technique, please see Ref [273]. In the last few years, research studies tracking soliton formation including single pulse formation [274–276], soliton molecule formation [277, 278] as well as harmonic mode-locking generation [279] in CNT-based fiber laser have made substantial advances owing to the DFT technique. The first demonstration of unveiling the entire buildup process from the relaxation oscillation into stable single soliton mode locking was reported by Liu's group in 2019 [275]. Previously, this group also investigated whole soliton molecule buildup evolution in detail in 2018 [277]. They also displayed the complete buildup evolution of HML in all-polarization-maintaining fiber CNT-based laser [279].

Except self-starting mode-locking dynamics, some extraordinarily rich ultrafast phenomena in CNT-based fiber laser have been investigated extensively, including soliton explosion [280], rogue wave generation [281], soliton pulsation [282, 283], the evolving soliton molecule

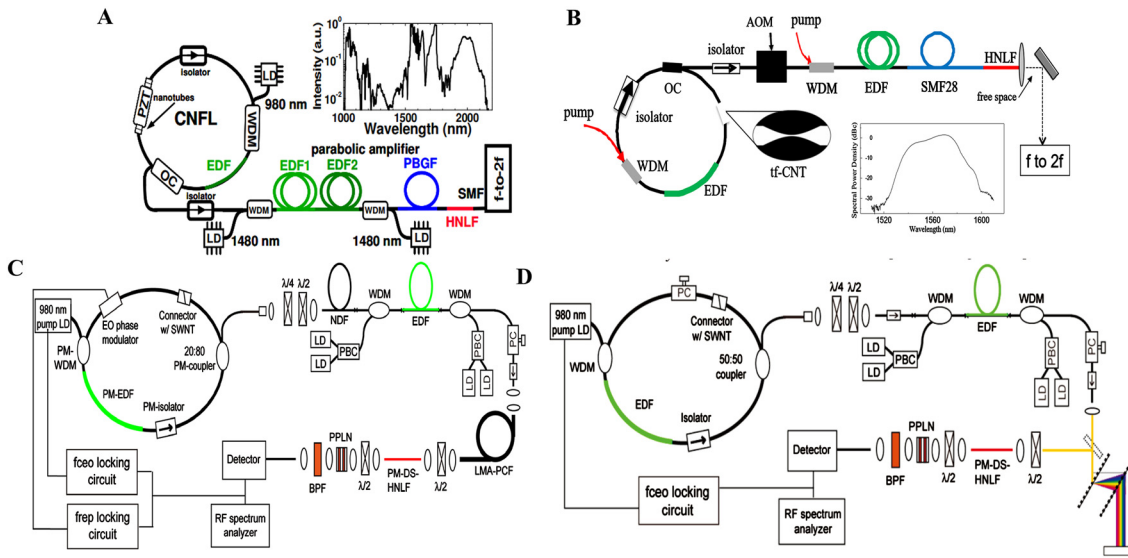


Figure 9: Typical experimental setup of OFC system using CNT SA mode-locked fiber laser.

(A) The first self-referenced frequency comb from a CNT mode-locked fiber laser. Lim et al. [253]. © Optical Society of America 2009. (B) A fiber frequency comb based on a tapered-fiber CNT design. Wu et al. [254]. © Optical Society of America 2011. (C) An OFC system based on an all-PM Er-doped fiber laser with SWNT PI film. Nishizawa et al. [259]. Author copyright. (D) An OFC system based on a dispersion managed Er-doped fiber laser with SWNT PI film. Nishizawa et al. [260]. Author copyright. CNT SA, carbon nanotube saturable absorber; OFC, optical frequency comb; SWNT PI, single walled carbon nanotube polyimide.

[284], etc. Unveiling the complex evolving dynamics can not only shed new light on the underlying physical mechanism but also can be conducive to optimize the cavity design. For a more comprehensive review on this subject, please see the recent publication in *Nanophotonics* [285].

Although the mode-locking dynamics of vector solitons in terms of buildup or propagation properties are of great interests to the community. In addition, the high flexibility in the control and generation of precessing state of polarization (SOP) can be also important in the context of trapping and manipulation of atoms and nanoparticles [286, 287], control of magnetization [288] and secure communications [289]. It is well known that the nonlinear pulse propagating in the mode-locked fiber lasers is vectorial owing to cavity anisotropy based on weekly irregular birefringence and randomly distributed CNT which suggests extra dimensionality of the pulse physical properties. Studies are devoted to the polarization dynamics to explore the correlation between nonlinear mechanism and laser dynamics [290–294]. However, phase difference and DOP may be overlooked by using conventional polarization beam splitter.

The trajectory of SOP, power of two orthogonal polarization component, phase difference and so forth can be obtained using commercial polarimeter. Typical polarization-locked vector solitons (PLVSs) and limited cycle attractor are shown in Figure 10. Figure 10A shows fixed point on Poincare sphere which indicates high DOP and stable SOP. Limited cycle shown in Figure 10B

represents the periodic modulation of anisotropy in the laser cavity corresponding to low DOP. Usually the real size of trajectories on the Poincare sphere may be larger than the measured trace owing to the limit of sampling rate of polarimeter. However, we can qualitatively estimate whether the trajectory is fixed point or not by DOP, which means the size of the trajectory covered area is inversely proportional to DOP. By adjusting pump power, polarization of pump power and the intracavity intrinsic birefringence, one can optimize the anisotropy in the cavity. The results of polarization precessing can be explained by the coupling between two cross-polarized SOP. In accordance with the theory of coupling oscillator, weak coupling between two cross-polarized SOP caused by isotropic cavity contributes to the complex behavior, such as spiral, double scroll [295]. Anisotropy of the cavity determined by the intrinsic birefringence and distribution of ions in the active medium may lead to a strong coupling, that is, a more stable state in the form of fixed point and limited cycle on the Poincare sphere.

In 2011, Mou et al. proposed a CNT-PVA thin film mode-locked erbium-doped fiber laser (EDFL) and observed the generation of polarization locked vector solitons [296, 297]. New families of vector soliton with locked and precessing states of polarization for multipulse soliton operations were comprehensively demonstrated [297]. Polarimeter with a higher resolution of 2 ns was applied to detect the soliton molecules with periodic polarization switching

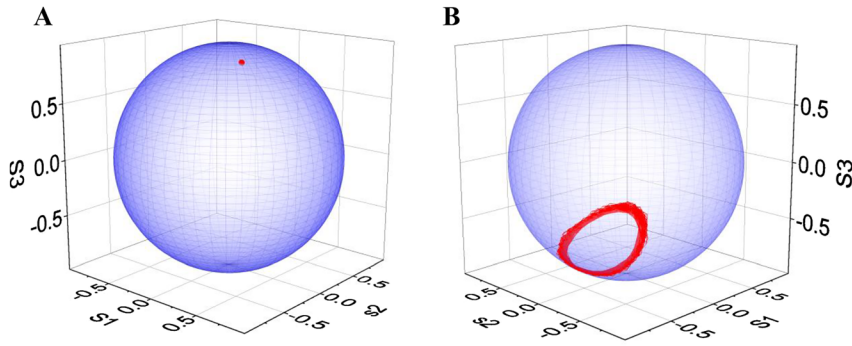


Figure 10: Typical fixed point and limited cycle shown in Poincare sphere. (A) Fixed point. (B) Limited cycle.

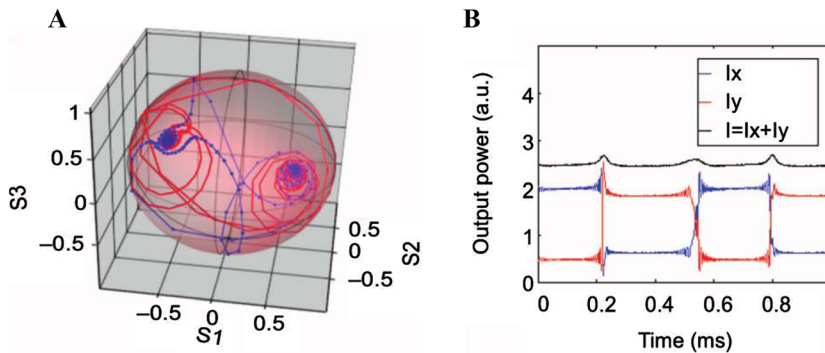


Figure 11: Results of double spiral attractors. (A) Polarization trajectory shown on Poincare sphere. (B) Power of two orthogonal polarization component. Sergeev et al. [295]. © CIOMP 2014.

between two and three SOPs and superposition of polarization switching with SOP precessing [298]. In 2013, it is shown that harmonic vector solitons with various orders by increasing pump power to explore the interplay between birefringence of the laser cavity created by polarization controller along with the pump light induced anisotropy caused by polarization hole burning [299]. Beyond the limit of nonlinear Schrodinger equations and Ginzburg Landau equations, Sergeev et al. demonstrated new vector model of EDFL accounted for the interaction between an optical field and an active medium to unveil the coupling between the two crossed polarization and experimentally observed a new type of polarization attractor as depicted in Figure 11 [295]. Double scroll attractor trajectory shown on Poincare sphere from Figure 11A can be proved from fractal dimensionality. Figure 11B exhibits powers of two linearly cross-polarized SOPs with periodic relaxation oscillation. The polarization dynamics of rogue waves were also studied to unveil the soliton–soliton and soliton–dispersive wave interactions. Bright-dark rogue waves were demonstrated experimentally caused by desynchronization of the orthogonal SOPs justified by a new model [300]. Vector soliton rain dynamics can be driven by polarization hole burning. By controlling the competition between polarization hole burning and refilling holes to control the soliton rain pulses evolution merging or repulsing [301], study on the polarization dynamics rogue waves helps in

exploring the origin of rogue waves. Recently, various polarization dynamics under dissipative solitons regime were observed which may help in unveiling a new type of high-energy ultrashort fiber lasers.

4 Conclusions and perspectives

The ongoing development of both CNT on the material side and applications in ultrafast fiber lasers are paving the future research of CNT mode-locked fiber lasers. From the material side, the purity of CNTs has been improved dramatically in the past decade. Nowadays, metallic tubes and semiconducting tubes can be separated properly [78]. Better control over chirality and diameter distribution can also be implemented. On the SA side, this offers more control and optimization on the absorption wavelength and linear loss of the CNT-based SAs. The mass production of CNT was not something new; this has secured a solid foundation for successful commercialization of CNT-based SAs. This may offer some comparative performance over popular SESAMs at some point. Indeed, from the early days, CNT-based mode-locked fiber lasers were commercialized. However, the underneath mass production of CNT-based SA has not been really implemented yet. We have noticed that some new method for fabricating CNT SAs using sol–gel was recently demonstrated [179].

Although in a very much early stage, the approach is promising in our perspective. We still recognized that the film-type CNT SAs could be an ideal method toward commercialization due to its similarity to semiconductor-based technology. Patterning, imprinting, slicing or even casting could be easily applied once a stable uniform CNT SA film will be obtained. Environmental-friendly polymers or other types of host material are still at large, provided some humidity-friendly SAs have been demonstrated already [302]. Emerging technologies such as inkjet printing could also allow large-scale fabrication of such nonlinear optical devices [303].

In terms of generating ultrashort pulses in a fiber laser, CNT SAs have routinely been utilized. It is well known that the electronic performance of CNT is superior. The recent demonstration of electric-controlled versatile pulse generation through a gated CNT film shows strong optoelectronic capability [304]. Moreover, well-aligned CNT samples based on various methods feature strong polarization-dependent optical absorption. The research revealed that SWNT SAs fabricated in zeolite single crystals will experience different nonlinear optical absorption against polarization of light, meanwhile influencing pulse generation [305], and this type of polarizer device based on aligned CNTs may have advantages in scalar soliton generation [306]. Rather than a conventional modulator device, such approaches could elevate the performance of ultrafast fiber lasers. In the future, we may expect some more powerful laser systems based on electronic, magnetic field or polarization-controlled versatile CNT SAs.

So far, CNTs have been demonstrated to mode-lock fiber lasers across a very broad wavelength range from visible to mid infrared. However, the gap around 1.7 μm has not been really fulfilled yet. This wavelength region is particularly interesting for biomedical imaging. The lack of good gain medium is also a key issue. On the other hand, one major obstacle for CNT SA development is the genuine short pulse duration generation. By far, the shorted pulse duration through a CNT mode-locked fiber laser is 66 fs in the telecom band [307]. While SESAM has been routinely applied to generate even few cycle pulses in a broad wavelength region, further optimization of CNT SAs for each wavelength window is still under investigation.

Apart from the fiber laser system, the excellent nonlinear optical absorption of CNTs has also been demonstrated in solid-state lasers for unique wavelength and applications. Another microcavity laser also gains enormous attention and the combination with CNT is increasingly meaningful and capable of opening up new research fields.

For future work, in general, a type of CNT SA could support high power endurance with mass production capability will be extremely interesting from our perspective. As this may trigger the CNT mode-locked fiber lasers to be a real milestone. Today, many more ultrafast laser sources do not rely on generation of short pulses only. Novel nonlinear schemes such as Mamyshev oscillator and spatial-temporal mode locking are not self-starting yet. CNT SAs may offer these new schemes a key to stability. Furthermore, we would like to see demonstrations of CNT SA mode-locked fiber lasers in the applications of XUV generation, tabletop accelerator, extreme low jitter source, etc.

Acknowledgments: This work was supported by the National Natural Science Foundation of China (NSFC) (61975107, 61605107). This work is also supported by the “111” project (D20031).

Author contribution: All the authors have accepted responsibility for the entire content of this submitted manuscript and approved submission.

Research funding: This research was funded by National Natural Science Foundation of China (NSFC) (61975107, 61605107), High Education Discipline Innovation Project (111 project) (D20031).

Conflict of interest statement: The authors declare no conflicts of interest regarding this article.

References

- [1] U. Keller, “Recent developments in compact ultrafast lasers,” *Nature*, vol. 424, pp. 831–838, 2003.
- [2] M. E. Fermann and I. Hartl, “Ultrafast fibre lasers,” *Nat. Photonics*, vol. 7, pp. 868–874, 2013.
- [3] A. Martinez and Z. Sun, “Nanotube and graphene saturable absorbers for fibre lasers,” *Nat. Photonics*, vol. 7, pp. 842–845, 2013.
- [4] L. Hou, H. Guo, Y. Wang, et al., “Sub-200 femtosecond dispersion-managed soliton ytterbium-doped fiber laser based on carbon nanotubes saturable absorber,” *Opt. Express*, vol. 26, pp. 9063–9070, 2018.
- [5] A. Tausenev, E. Obraztsova, A. Lobach, et al., “177 fs erbium-doped fiber laser mode locked with a cellulose polymer film containing single-wall carbon nanotubes,” *Appl. Phys. Lett.*, vol. 92, p. 171113, 2008.
- [6] Y. Wang, S.-U. Alam, E. D. Obraztsova, et al., “Generation of stretched pulses and dissipative solitons at 2 μm from an all-fiber mode-locked laser using carbon nanotube saturable absorbers,” *Opt. Lett.*, vol. 41, pp. 3864–3867, 2016.
- [7] C. Wei, Y. Lyu, H. Shi, et al., “Mid-Infrared Q-switched and mode-locked fiber lasers at 2.87 μm based on carbon nanotube,” *IEEE J. Sel. Top. Quant. Electron.*, vol. 25, pp. 1–6, 2019.

- [8] U. Willer, M. Saraji, A. Khorsandi, et al., “Near-and mid-infrared laser monitoring of industrial processes, environment and security applications,” *Opt. Laser Eng.*, vol. 44, pp. 699–710, 2006.
- [9] N. M. Fried, “Thulium fiber laser lithotripsy: An in vitro analysis of stone fragmentation using a modulated 110-watt Thulium fiber laser at 1.94 μm . Lasers in Surgery and Medicine,” *Off. J. Am. Soc. Laser Med. Surg.* vol. 37, pp. 53–58, 2005.
- [10] J. Wang, Y. Chen, and W. J. Blau, “Carbon nanotubes and nanotube composites for nonlinear optical devices,” *J. Mater. Chem.*, vol. 19, pp. 7425–7443, 2009.
- [11] Z. Huang, Q. Huang, A. Theodosiou, et al., “All-fiber passively mode-locked ultrafast laser based on a femtosecond-laser-inscribed in-fiber Brewster device,” *Opt. Lett.*, vol. 44, pp. 5177–5180, 2019.
- [12] J. Liu, Y. Chen, P. Tang, et al., “Generation and evolution of mode-locked noise-like square-wave pulses in a large-anomalous-dispersion Er-doped ring fiber laser,” *Opt. Express*, vol. 23, pp. 6418–6427, 2015.
- [13] W. Pan, J. Zhou, L. Zhang, and Y. Feng, “Raman dissipative soliton fiber laser mode locked by a nonlinear optical loop mirror,” *Opt. Express*, vol. 27, pp. 17905–17911, 2019.
- [14] D. Kim, D. Kwon, B. Lee, and J. Kim, “Polarization-maintaining nonlinear-amplifying-loop-mirror mode-locked fiber laser based on a 3×3 coupler,” *Opt. Lett.*, vol. 44, pp. 1068–1071, 2019.
- [15] X. Liu, Y. Cui, D. Han, X. Yao, and Z. Sun, “Distributed ultrafast fibre laser,” *Sci. Rep.*, vol. 5, p. 9101, 2015.
- [16] X. Liu, D. Han, Z. Sun, et al., “Versatile multi-wavelength ultrafast fiber laser mode-locked by carbon nanotubes,” *Sci. Rep.*, vol. 3, p. 2718, 2013.
- [17] Z. Chen, H. Wang, Y. Wang, et al., “Improved optical damage threshold graphene Oxide/SiO₂ absorber fabricated by sol-gel technique for mode-locked erbium-doped fiber lasers,” *Carbon*, vol. 144, pp. 737–744, 2019.
- [18] J. E. Moore, “The birth of topological insulators,” *Nature*, vol. 464, pp. 194–198, 2010.
- [19] H. Zhang, C.-X. Liu, X.-L. Qi, et al., “Topological insulators in Bi₂Se₃, Bi₂Te₃ and Sb₂Te₃ with a single Dirac cone on the surface,” *Nat. Phys.*, vol. 5, pp. 438–442, 2009.
- [20] K. F. Mak, and J. Shan, “Photonics and optoelectronics of 2D semiconductor transition metal dichalcogenides,” *Nat. Photonics*, vol. 10, pp. 216–226, 2016.
- [21] T. Jiang, K. Yin, C. Wang, et al., “Ultrafast fiber lasers mode-locked by two-dimensional materials: review and prospect,” *Photonics Res.*, vol. 8, pp. 78–90, 2020.
- [22] Y. Ge, Z. Zhu, Y. Xu, et al., “Broadband nonlinear photoresponse of 2D TiS₂ for ultrashort pulse generation and all-optical thresholding devices,” *Adv. Opt. Mater.*, vol. 6, p. 1701166, 2018.
- [23] J. He, L. Tao, H. Zhang, B. Zhou, and J. Li, “Emerging 2D materials beyond graphene for ultrashort pulse generation in fiber lasers,” *Nanoscale*, vol. 11, pp. 2577–2593, 2019.
- [24] F. Xia, H. Wang, and Y. Jia, “Rediscovering black phosphorus as an anisotropic layered material for optoelectronics and electronics,” *Nat. Commun.*, vol. 5, pp. 1–6, 2014.
- [25] M. Buscema, D. J. Groenendijk, S. I. Blanter, et al., “Fast and broadband photoresponse of few-layer black phosphorus field-effect transistors,” *Nano Lett.*, vol. 14, pp. 3347–3352, 2014.
- [26] M. Zhang, Q. Wu, F. Zhang, et al., “2D black phosphorus saturable absorbers for ultrafast photonics,” *Adv. Opt. Mater.*, vol. 7, p. 1800224, 2019.
- [27] J. Pei, J. Yang, T. Yildirim, H. Zhang, and Y. Lu, “Many-body complexes in 2D semiconductors,” *Adv. Mater.*, vol. 31, p. 1706945, 2019.
- [28] Y. Song, S. Chen, Q. Zhang, et al., “Vector soliton fiber laser passively mode locked by few layer black phosphorus-based optical saturable absorber,” *Opt. Express*, vol. 24, pp. 25933–25942, 2016.
- [29] Y. Dong, S. Chertopalov, K. Maleski, et al., “Saturable absorption in 2D Ti₃C₂ MXene thin films for passive photonic diodes,” *Adv. Mater.*, vol. 30, p. 1705714, 2018.
- [30] X. Jiang, A. V. Kuklin, A. Baev, et al., “Two-dimensional MXenes: from morphological to optical, electric, and magnetic properties and applications,” *Phys. Rep.*, vol. 848, pp. 1–58, 2020.
- [31] E. Aktürk, O. Ü. Aktürk, and S. Ciraci, “Single and bilayer bismuthene: stability at high temperature and mechanical and electronic properties,” *Phys. Rev. B*, vol. 94, p. 014115, 2016.
- [32] B. Guo, S.-H. Wang, Z.-X. Wu, et al., “Sub-200 fs soliton mode-locked fiber laser based on bismuthene saturable absorber,” *Opt. Express*, vol. 26, pp. 22750–22760, 2018.
- [33] T. Chai, X. Li, T. Feng, et al., “Few-layer bismuthene for ultrashort pulse generation in a dissipative system based on an evanescent field,” *Nanoscale*, vol. 10, pp. 17617–17622, 2018.
- [34] M. Pumera and Z. Sofer, “2D mono-elemental arsenene, antimonene, and bismuthene: beyond black phosphorus,” *Adv. Mater.*, vol. 29, p. 1605299, 2017.
- [35] Y. Song, Z. Liang, X. Jiang, et al., “Few-layer antimonene decorated microfiber: ultra-short pulse generation and all-optical thresholding with enhanced long term stability,” *2D Mater.*, vol. 4, p. 045010, 2017.
- [36] P. Li, Y. Chen, T. Yang, et al., “Two-dimensional CH₃NH₃PbI₃ perovskite nanosheets for ultrafast pulsed fiber lasers,” *ACS Appl. Mater. Interfaces*, vol. 9, pp. 12759–12765, 2017.
- [37] Y. Zhang, C.-K. Lim, Z. Dai, et al., “Photonics and optoelectronics using nano-structured hybrid perovskite media and their optical cavities,” *Phys. Rep.*, vol. 795, pp. 1–51, 2019.
- [38] X. Qi, Y. Zhang, Q. Ou, et al., “Photonics and optoelectronics of 2D metal-halide perovskites,” *Small*, vol. 14, p. 1800682, 2018.
- [39] W. Zhang, L. Zhan, T. Xian, and L. Gao, “Bidirectional dark-soliton fiber lasers for high-sensitivity gyroscopic application,” *Opt. Lett.*, vol. 44, pp. 4008–4011, 2019.
- [40] K. Zhao, Y. Li, X. Xiao, and C. Yang, “Nonlinear multimode interference-based dual-color mode-locked fiber laser,” *Opt. Lett.*, vol. 45, pp. 1655–1658, 2020.
- [41] Z. Wang, L. Zhan, J. Wu, et al., “Self-starting ultrafast fiber lasers mode-locked with alcohol,” *Opt. Lett.*, vol. 40, pp. 3699–3702, 2015.
- [42] T. Xian, L. Zhan, L. Gao, W. Zhang, and W. Zhang, “Passively Q-switched fiber lasers based on pure water as the saturable absorber,” *Opt. Lett.*, vol. 44, pp. 863–866, 2019.
- [43] P. Cheng, Y. Du, M. Han, and X. Shu, “Mode-locked and Q-switched mode-locked fiber laser based on a ferroferric-oxide nanoparticles saturable absorber,” *Opt. Express*, vol. 28, pp. 13177–13186, 2020.

- [44] Y. Ge, W. Huang, F. Yang, et al., “Beta-lead oxide quantum dot (β -PbO QD)/polystyrene (PS) composite films and their applications in ultrafast photonics,” *Nanoscale*, vol. 11, pp. 6828–6837, 2019.
- [45] J. Du, M. Zhang, Z. Guo, et al., “Phosphorene quantum dot saturable absorbers for ultrafast fiber lasers,” *Sci. Rep.*, vol. 7, p. 42357, 2017.
- [46] Y.-C. Chen, N. Ravikiran, L. Schadler, et al., “Ultrafast optical switching properties of single-wall carbon nanotube polymer composites at 1.55 μm ,” *Appl. Phys. Lett.*, vol. 81, pp. 975–977, 2002.
- [47] G. Ostojic, S. Zaric, J. Kono, et al., “Interband recombination dynamics in resonantly excited single-walled carbon nanotubes,” *Phys. Rev. Lett.*, vol. 92, p. 117402, 2004.
- [48] S. Set, H. Yaguchi, Y. Tanaka, et al., “Mode-locked fiber lasers based on a saturable absorber incorporating carbon nanotubes,” in *Optical Fiber Communication Conference*, Optical Society of America, 2003, p. PD44.
- [49] T. Hasan, Z. Sun, F. Wang, et al., “Nanotube–polymer composites for ultrafast photonics,” *Adv. Mater.*, vol. 21, pp. 3874–3899, 2009.
- [50] M. Chernysheva, A. Rozhin, Y. Fedotov, et al., “Carbon nanotubes for ultrafast fibre lasers,” *Nanophotonics*, vol. 6, pp. 1–30, 2017.
- [51] H. Chu, Y. Li, C. Wang, H. Zhang, and D. Li, “Recent investigations on nonlinear absorption properties of carbon nanotubes,” *Nanophotonics*, vol. 9, pp. 761–781, 2020.
- [52] C. E. Baddour and C. Briens, “Carbon nanotube synthesis: A review,” *Int. J. Chem. React. Eng.*, vol. 3, pp. 1–20, 2005.
- [53] F. H. Hussein and F. H. Abdulrazzak, “Synthesis of carbon nanotubes by chemical vapor deposition,” in *Nanomaterials: Biomedical, Environmental, and Engineering Applications*, New York, John Wiley and Sons, 2018, pp. 105–132, <https://doi.org/10.1002/9781119370383>.
- [54] E. Joselevich, H. Dai, J. Liu, K. Hata, and A. H. Windle, “Carbon Nanotube Synthesis and Organization,” in *Carbon Nanotube Synthesis and Organization. Carbon Nanotubes*, Berlin, Heidelberg, Springer, 2007, pp. 101–165.
- [55] M. Kumar and Y. Ando, “Chemical vapor deposition of carbon nanotubes: A review on growth mechanism and mass production,” *J. Nanosci. Nanotechnol.*, vol. 10, pp. 3739–3758, 2010.
- [56] J. Sengupta, “Carbon nanotube fabrication at industrial scale: Opportunities and challenges,” in *Handbook of Nanomaterials for Industrial Applications*, Amsterdam (Netherlands), Elsevier, 2018, pp. 172–194.
- [57] K. A. Shah, and B. A. Tali, “Synthesis of carbon nanotubes by catalytic chemical vapour deposition: A review on carbon sources, catalysts and substrates,” *Mater. Sci. Semicond. Process.*, vol. 41, pp. 67–82, 2016.
- [58] X.-D. Wang, K. Vinodgopal, and G.-P. Dai, *Synthesis of Carbon Nanotubes by Catalytic Chemical Vapor Deposition. Perspective of Carbon Nanotubes*, London, UK, IntechOpen, 2019.
- [59] J. R. Sanchez-Valencia, T. Dienel, O. Gröning, et al., “Controlled synthesis of single-chirality carbon nanotubes,” *Nature*, vol. 512, pp. 61–64, 2014.
- [60] H. Wang, Y. Yuan, L. Wei, et al., “Catalysts for chirality selective synthesis of single-walled carbon nanotubes,” *Carbon*, vol. 81, pp. 1–19, 2015.
- [61] R. Rao, D. Liptak, T. Cherukuri, B. I. Yakobson, and B. Maruyama, “In situ evidence for chirality-dependent growth rates of individual carbon nanotubes,” *Nat. Mater.*, vol. 11, pp. 213–216, 2012.
- [62] J. Tomada, T. Dienel, F. Hampel, R. Fasel, and K. Amsharov, “Combinatorial design of molecular seeds for chirality-controlled synthesis of single-walled carbon nanotubes,” *Nat. Commun.*, vol. 10, pp. 1–10, 2019.
- [63] M. Ahmed, N. Ali, Z. Salleh, et al., “Q-switched erbium doped fiber laser based on single and multiple walled carbon nanotubes embedded in polyethylene oxide film as saturable absorber,” *Opt. Laser. Technol.*, vol. 65, pp. 25–28, 2015.
- [64] M. Chernysheva, A. Bednyakova, M. Al Araimi, et al., “Double-wall carbon nanotube hybrid mode-locker in tm-doped fibre laser: A novel mechanism for robust bound-state solitons generation,” *Sci. Rep.*, vol. 7, p. 44314, 2017.
- [65] T. Hasan, Z. Sun, P. Tan, et al., “Double-wall carbon nanotubes for wide-band, ultrafast pulse generation,” *ACS Nano*, vol. 8, pp. 4836–4847, 2014.
- [66] M. S. Arnold, J. E. Sharping, S. I. Stupp, P. Kumar, and M. C. Hersam, “Band gap photobleaching in isolated single-walled carbon nanotubes,” *Nano Lett.*, vol. 3, pp. 1549–1554, 2003.
- [67] S. Y. Set, H. Yaguchi, Y. Tanaka, and M. Jablonski, “Ultrafast fiber pulsed lasers incorporating carbon nanotubes,” *IEEE J. Sel. Top. Quant. Electron.*, vol. 10, pp. 137–146, 2004.
- [68] S. Xu, F. Wang, C. Zhu, et al., “Ultrafast nonlinear photoresponse of single-wall carbon nanotubes: A broadband degenerate investigation,” *Nanoscale*, vol. 8, pp. 9304–9309, 2016.
- [69] M. Ouyang, J.-L. Huang, C. L. Cheung, and C. M. Lieber, “Energy gaps in “metallic” single-walled carbon nanotubes,” *Science*, vol. 292, pp. 702–705, 2001.
- [70] C. D. Spataru, S. Ismail-Beigi, L. X. Benedict, and S. G. Louie, “Excitonic effects and optical spectra of single-walled carbon nanotubes,” *Phys. Rev. Lett.*, vol. 92, p. 077402, 2004.
- [71] L. Lüer, G. Lanzani, J. Crochet, et al., “Ultrafast dynamics in metallic and semiconducting carbon nanotubes,” *Phys. Rev. B*, vol. 80, p. 205411, 2009.
- [72] J. Shi, H. Chu, Y. Li, et al., “Synthesis and nonlinear optical properties of semiconducting single-walled carbon nanotubes at 1 μm ,” *Nanoscale*, vol. 11, pp. 7287–7292, 2019.
- [73] X. Zhang, S. Zhao, Y. Li, et al., “Liquid-phase exfoliated semiconducting single-walled carbon nanotubes as a saturable absorber for passively Q-switched laser,” *J. Nanophotonics*, vol. 12, p. 026020, 2018.
- [74] M. Pawliszewska, A. Dużyńska, M. Zdrojek, and J. Sotor, “Metallic carbon nanotube-based saturable absorbers for holmium-doped fiber lasers,” *Opt. Express*, vol. 27, pp. 11361–11369, 2019.
- [75] W.-J. Kim, M. L. Usrey, and M. S. Strano, “Selective functionalization and free solution electrophoresis of single-walled carbon nanotubes: separate enrichment of metallic and semiconducting SWNT,” *Chem. Mater.*, vol. 19, pp. 1571–1576, 2007.
- [76] R. Krupke, F. Hennrich, H. V. Löhneysen, and M. M. Kappes, “Separation of metallic from semiconducting single-walled carbon nanotubes,” *Science*, vol. 301, pp. 344–347, 2003.
- [77] M. S. Arnold, S. I. Stupp, and M. C. Hersam, “Enrichment of single-walled carbon nanotubes by diameter in density gradients,” *Nano Lett.*, vol. 5, pp. 713–718, 2005.
- [78] M. S. Arnold, A. A. Green, J. F. Hulvat, S. I. Stupp, and M. C. Hersam, “Sorting carbon nanotubes by electronic structure

- using density differentiation,” *Nat. Nanotechnol.*, vol. 1, pp. 60–65, 2006.
- [79] K. Yanagi, T. Iitsuka, S. Fujii, and H. Kataura, “Separations of metallic and semiconducting carbon nanotubes by using sucrose as a gradient medium,” *J. Phys. Chem. C*, vol. 112, pp. 18889–18894, 2008.
- [80] E. J. Carvalho and M. C. dos Santos, “Role of surfactants in carbon nanotubes density gradient separation,” *ACS Nano*, vol. 4, pp. 765–770, 2010.
- [81] P. Zhao, E. Einarsson, R. Xiang, Y. Murakami, and S. Maruyama, “Controllable expansion of single-walled carbon nanotube dispersions using density gradient ultracentrifugation,” *J. Phys. Chem. C*, vol. 114, pp. 4831–4834, 2010.
- [82] P. Zhao, E. Einarsson, G. Lagoudas, et al., “Tunable separation of single-walled carbon nanotubes by dual-surfactant density gradient ultracentrifugation,” *Nano Res*, vol. 4, pp. 623–634, 2011.
- [83] X. Tu, S. Manohar, A. Jagota, and M. Zheng, “DNA sequence motifs for structure-specific recognition and separation of carbon nanotubes,” *Nature*, vol. 460, pp. 250–253, 2009.
- [84] H. Kataura, Y. Kumazawa, Y. Maniwa, et al., “Optical properties of single-wall carbon nanotubes,” *Synth. Met.*, vol. 103, pp. 2555–2558, 1999.
- [85] O. Lourie, D. Cox, and H. Wagner, “Buckling and collapse of embedded carbon nanotubes,” *Phys. Rev. Lett.*, vol. 81, p. 1638, 1998.
- [86] A. Thess, R. Lee, P. Nikolaev, et al., “Crystalline ropes of metallic carbon nanotubes,” *Science*, vol. 273, pp. 483–487, 1996.
- [87] L. Girifalco, M. Hodak, and R. S. Lee, “Carbon nanotubes, buckyballs, ropes, and a universal graphitic potential,” *Phys. Rev. B*, vol. 62, p. 13104, 2000.
- [88] L. Vaisman, H. D. Wagner, and G. Marom, “The role of surfactants in dispersion of carbon nanotubes,” *Adv. Colloid Interface Sci.*, vol. 128, pp. 37–46, 2006.
- [89] P.-C. Ma, N. A. Siddiqui, G. Marom, and J.-K. Kim, “Dispersion and functionalization of carbon nanotubes for polymer-based nanocomposites: A review,” *Compos. Part A Appl. Sci. Manuf.*, vol. 41, pp. 1345–1367, 2010.
- [90] J. Hilding, E. A. Grulke, Z. George Zhang, and F. Lockwood, “Dispersion of carbon nanotubes in liquids,” *J. Dispersion Sci. Technol.*, vol. 24, pp. 1–41, 2003.
- [91] Y. Y. Huang and E. M. Terentjev, “Dispersion of carbon nanotubes: mixing, sonication, stabilization, and composite properties,” *Polymers*, vol. 4, pp. 275–295, 2012.
- [92] S. W. Kim, T. Kim, Y. S. Kim, et al., “Surface modifications for the effective dispersion of carbon nanotubes in solvents and polymers,” *Carbon*, vol. 50, pp. 3–33, 2012.
- [93] O. V. Kharissova and B. I. Kharisov, *Solubilization and Dispersion of Carbon Nanotubes*, Cham. Switzerland, Springer, 2017.
- [94] S. Manzetti and J.-C. P. Gabriel, “Methods for dispersing carbon nanotubes for nanotechnology applications: liquid nanocrystals, suspensions, polyelectrolytes, colloids and organization control,” *Int. Nano Lett.*, vol. 9, pp. 31–49, 2019.
- [95] K. Yang, Z. Yi, Q. Jing, et al., “Sonication-assisted dispersion of carbon nanotubes in aqueous solutions of the anionic surfactant SDBS: the role of sonication energy,” *Chin. Sci. Bull.*, vol. 58, pp. 2082–2090, 2013.
- [96] V. Tarasov, M. Komkov, N. Stepanishchev, V. Romanenkov, and R. Boyarskaya, “Modification of polyester resin binder by carbon nanotubes using ultrasonic dispersion,” *Polym. Sci. Ser. D*, vol. 8, pp. 9–16, 2015.
- [97] V. C. Moore, M. S. Strano, E. H. Haroz, et al., “Individually suspended single-walled carbon nanotubes in various surfactants,” *Nano Lett.*, vol. 3, pp. 1379–1382, 2003.
- [98] W. C. Herndon, “The structure of choleic acids,” *J. Chem. Educ.*, vol. 44, p. 724, 1967.
- [99] M. Islam, E. Rojas, D. Bergey, A. Johnson, and A. Yodh, “High weight fraction surfactant solubilization of single-wall carbon nanotubes in water,” *Nano Lett.*, vol. 3, pp. 269–273, 2003.
- [100] M. J. O’connell, S. M. Bachilo, C. B. Huffman, et al., “Band gap fluorescence from individual single-walled carbon nanotubes,” *Science*, vol. 297, pp. 593–596, 2002.
- [101] R. M. Fernandes, B. Abreu, B. Claro, et al., “Dispersing carbon nanotubes with ionic surfactants under controlled conditions: comparisons and insight,” *Langmuir*, vol. 31, pp. 10955–10965, 2015.
- [102] J. C. Goak, S. H. Lee, J. H. Han, et al., “Spectroscopic studies and electrical properties of transparent conductive films fabricated by using surfactant-stabilized single-walled carbon nanotube suspensions,” *Carbon*, vol. 49, pp. 4301–4313, 2011.
- [103] H. Gui, H. Chen, C. Y. Khripin, et al., “A facile and low-cost length sorting of single-wall carbon nanotubes by precipitation and applications for thin-film transistors,” *Nanoscale*, vol. 8, pp. 3467–3473, 2016.
- [104] T. Chatterjee, K. Yurekli, V. G. Hadjiev, and R. Krishnamoorti, “Single-walled carbon nanotube dispersions in poly (ethylene oxide),” *Adv. Funct. Mater.*, vol. 15, pp. 1832–1838, 2005.
- [105] W. Wenseleers, I. I. Vlasov, E. Goovaerts, et al., “Efficient isolation and solubilization of pristine single-walled nanotubes in bile salt micelles,” *Adv. Funct. Mater.*, vol. 14, pp. 1105–1112, 2004.
- [106] Y. Tan and D. E. Resasco, “Dispersion of single-walled carbon nanotubes of narrow diameter distribution,” *J. Phys. Chem. B*, vol. 109, pp. 14454–14460, 2005.
- [107] R. Haggemueller, S. S. Rahatekar, J. A. Fagan, et al., “Comparison of the quality of aqueous dispersions of single wall carbon nanotubes using surfactants and biomolecules,” *Langmuir*, vol. 24, pp. 5070–5078, 2008.
- [108] T. H. Kim, C. Doe, S. R. Kline, and S. M. Choi, “Water-redispersible isolated single-walled carbon nanotubes fabricated by in situ polymerization of micelles,” *Adv. Mater.*, vol. 19, pp. 929–933, 2007.
- [109] N. A. Monteiro-Riviere, A. O. Inman, Y. Y. Wang, and R. J. Nemanich, “Surfactant effects on carbon nanotube interactions with human keratinocytes,” *Nanomedicine*, vol. 1, pp. 293–299, 2005.
- [110] L. Vaisman, G. Marom, and H. D. Wagner, “Dispersions of surface-modified carbon nanotubes in water-soluble and water-insoluble polymers,” *Adv. Funct. Mater.*, vol. 16, pp. 357–363, 2006.
- [111] X. Gong, J. Liu, S. Baskaran, R. D. Voise, and J. S. Young, “Surfactant-assisted processing of carbon nanotube/polymer composites,” *Chem. Mater.*, vol. 12, pp. 1049–1052, 2000.
- [112] S. Cui, R. Canet, A. Derre, M. Couzi, and P. Delhaes, “Characterization of multiwall carbon nanotubes and influence

- of surfactant in the nanocomposite processing,” *Carbon*, vol. 41, pp. 797–809, 2003.
- [113] M. S. Strano, V. C. Moore, M. K. Miller, et al., “The role of surfactant adsorption during ultrasonication in the dispersion of single-walled carbon nanotubes,” *J. Nanosci. Nanotechnol.*, vol. 3, pp. 81–86, 2003.
- [114] D. Kim, T. Lee, M. Kwon, et al., “Polymer wrapping-induced dispersion of single walled carbon nanotubes in ethylene glycol under mild sonication,” *RSC Adv.*, vol. 10, pp. 26262–26267, 2020.
- [115] H.-J. Butt, K. Graf, and M. Kappl, *Physics and Chemistry of Interfaces*, New York, John Wiley & Sons, 2013.
- [116] K. Yurekli, C. A. Mitchell, and R. Krishnamoorti, “Small-angle neutron scattering from surfactant-assisted aqueous dispersions of carbon nanotubes,” *J. Am. Chem. Soc.*, vol. 126, pp. 9902–9903, 2004.
- [117] A. Yu, C.-C. L. Su, I. Roes, B. Fan, and R. C. Haddon, “Gram-scale preparation of surfactant-free, carboxylic acid groups functionalized, individual single-walled carbon nanotubes in aqueous solution,” *Langmuir*, vol. 26, pp. 1221–1225, 2010.
- [118] H. Kato, K. Mizuno, M. Shimada, et al., “Observations of bound Tween80 surfactant molecules on single-walled carbon nanotubes in an aqueous solution,” *Carbon*, vol. 47, pp. 3434–3440, 2009.
- [119] P.-C. Ma, N. A. Siddiqui, E. Mäder, and J.-K. Kim, “Correlation between electrokinetic potential, dispersibility, surface chemistry and energy of carbon nanotubes,” *Compos. Sci. Technol.*, vol. 71, pp. 1644–1651, 2011.
- [120] Z. Sun, V. Nicolosi, D. Rickard, et al., “Quantitative evaluation of surfactant-stabilized single-walled carbon nanotubes: dispersion quality and its correlation with zeta potential,” *J. Phys. Chem. C*, vol. 112, pp. 10692–10699, 2008.
- [121] S. Giordani, S. D. Bergin, V. Nicolosi, et al., “Debundling of single-walled nanotubes by dilution: observation of large populations of individual nanotubes in amide solvent dispersions,” *J. Phys. Chem. B*, vol. 110, pp. 15708–15718, 2006.
- [122] K. D. Ausman, R. Piner, O. Lourie, R. S. Ruoff, and M. Korobov, “Organic solvent dispersions of single-walled carbon nanotubes: toward solutions of pristine nanotubes,” *J. Phys. Chem. B*, vol. 104, pp. 8911–8915, 2000.
- [123] B. J. Landi, H. J. Ruf, J. J. Worman, and R. P. Raffaele, “Effects of alkyl amide solvents on the dispersion of single-wall carbon nanotubes,” *J. Phys. Chem. B*, vol. 108, pp. 17089–17095, 2004.
- [124] T. Hasan, V. Scardaci, P. Tan, et al., “Stabilization and “debundling” of single-wall carbon nanotube dispersions in N-methyl-2-pyrrolidone (NMP) by polyvinylpyrrolidone (PVP),” *J. Phys. Chem. C*, vol. 111, pp. 12594–12602, 2007.
- [125] J. L. Bahr, E. T. Mickelson, M. J. Bronikowski, R. E. Smalley, and J. M. Tour, “Dissolution of small diameter single-wall carbon nanotubes in organic solvents?,” *Chem. Commun.*, vol. 2, pp. 193–194, 2001.
- [126] R. Krupke, F. Hennrich, O. Hampe, and M. M. Kappes, “Near-infrared absorbance of single-walled carbon nanotubes dispersed in dimethylformamide,” *J. Phys. Chem. B*, vol. 107, pp. 5667–5669, 2003.
- [127] S. D. Bergin, V. Nicolosi, P. V. Streich, et al., “Towards solutions of single-walled carbon nanotubes in common solvents,” *Adv. Mater.*, vol. 20, pp. 1876–1881, 2008.
- [128] T. Hasan, P. Tan, F. Bonaccorso, et al., “Polymer-Assisted isolation of single wall carbon nanotubes in organic solvents for optical-quality Nanotube– polymer composites,” *J. Phys. Chem. C*, vol. 112, pp. 20227–20232, 2008.
- [129] T. Hasan, V. Scardaci, P. Tan, et al., “Dispersibility and stability improvement of unfunctionalized nanotubes in amide solvents by polymer wrapping,” *Physica E Low Dimens. Syst. Nanostruct.*, vol. 40, pp. 2414–2418, 2008.
- [130] S. Attal, R. Thiruvengadathan, and O. Regev, “Determination of the concentration of single-walled carbon nanotubes in aqueous dispersions using UV– Visible absorption spectroscopy,” *Anal. Chem.*, vol. 78, pp. 8098–8104, 2006.
- [131] J. Njuguna, O. A. Vanli, and R. Liang, “A review of spectral methods for dispersion characterization of carbon nanotubes in aqueous suspensions,” *J. Spectrosc. (Hindawi)*, vol. 2015, pp. 463156, 2015.
- [132] B. Yang, L. Ren, L. Li, et al., “The characterization of the concentration of the single-walled carbon nanotubes in aqueous dispersion by UV-Vis-NIR absorption spectroscopy,” *Analyst*, vol. 138, pp. 6671–6676, 2013.
- [133] M.-C. D. Yang, M.-Y. Li, S. Luo, and R. Liang, “Real-time monitoring of carbon nanotube dispersion using dynamic light scattering and UV-vis spectroscopy,” *Int. J. Adv. Manuf. Technol.*, vol. 82, pp. 361–367, 2016.
- [134] M. Sheik-Bahae, A. A. Said, and E. W. Van Stryland, “High-sensitivity, single-beam n_2 measurements,” *Opt. Lett.*, vol. 14, pp. 955–957, 1989.
- [135] M. Sheik-Bahae, A. A. Said, T.-H. Wei, D. J. Hagan, and E. W. Van Stryland, “Sensitive measurement of optical nonlinearities using a single beam,” *IEEE J. Quant. Electron.*, vol. 26, pp. 760–769, 1990.
- [136] P. Chapple, J. Staromlynska, and R. McDuff, “Z-scan studies in the thin-and the thick-sample limits,” *J. Opt. Soc. Am. B*, vol. 11, pp. 975–982, 1994.
- [137] J.-M. Ménard, M. Betz, I. Sigal, and H. M. van Driel, “Single-beam differential z-scan technique,” *Appl. Opt.*, vol. 46, pp. 2119–2122, 2007.
- [138] S. Niyogi, S. Boukhalfa, S. B. Chikkannanavar, et al., “Selective aggregation of single-walled carbon nanotubes via salt addition,” *J. Am. Chem. Soc.*, vol. 129, pp. 1898–1899, 2007.
- [139] P. Tan, A. Rozhin, T. Hasan, et al., “Photoluminescence spectroscopy of carbon nanotube bundles: evidence for exciton energy transfer,” *Phys. Rev. Lett.*, vol. 99, p. 137402, 2007.
- [140] T. J. McDonald, C. Engtrakul, M. Jones, G. Rumbles, and M. J. Heben, “Kinetics of PL quenching during single-walled carbon nanotube rebundling and diameter-dependent surfactant interactions,” *J. Phys. Chem. B*, vol. 110, pp. 25339–25346, 2006.
- [141] H. Cathcart, S. Quinn, V. Nicolosi, et al., “Spontaneous debundling of single-walled carbon nanotubes in DNA-based dispersions,” *J. Phys. Chem. C*, vol. 111, pp. 66–74, 2007.
- [142] P. Tan, T. Hasan, F. Bonaccorso, et al., “Optical properties of nanotube bundles by photoluminescence excitation and absorption spectroscopy,” *Physica E Low Dimens. Syst. Nanostruct.*, vol. 40, pp. 2352–2359, 2008.
- [143] J. Crochet, M. Clemens, and T. Hertel, “Quantum yield heterogeneities of aqueous single-wall carbon nanotube suspensions,” *J. Am. Chem. Soc.*, vol. 129, pp. 8058–8059, 2007.

- [144] A. Gambetta, G. Galzerano, A. Rozhin, et al., “Sub-100 fs two-color pump-probe spectroscopy of single wall carbon nanotubes with a 100 MHz Er-fiber laser system,” *Opt. Express*, vol. 16, pp. 11727–11734, 2008.
- [145] O. Korovyanko, C.-X. Sheng, Z. Vardeny, A. Dalton, and R. Baughman, “Ultrafast spectroscopy of excitons in single-walled carbon nanotubes,” *Phys. Rev. Lett.*, vol. 92, p. 017403, 2004.
- [146] M. S. Dresselhaus, G. Dresselhaus, R. Saito, and A. Jorio, “Raman spectroscopy of carbon nanotubes,” *Phys. Rep.*, vol. 409, pp. 47–99, 2005.
- [147] M. Dresselhaus, G. Dresselhaus, A. Jorio, A. Souza Filho, and R. Saito, “Raman spectroscopy on isolated single wall carbon nanotubes,” *Carbon*, vol. 40, pp. 2043–2061, 2002.
- [148] M. Chernysheva, M. Al Araiimi, G. A. Rance, et al., “Revealing the nature of morphological changes in carbon nanotube-polymer saturable absorber under high-power laser irradiation,” *Sci. Rep.*, vol. 8, pp. 1–9, 2018.
- [149] A. Jorio, A. Santos, H. Ribeiro, et al., “Quantifying carbon-nanotube species with resonance Raman scattering,” *Phys. Rev. B Condens. Matter*, vol. 72, p. 075207, 2005.
- [150] A. Jungen, V. N. Popov, C. Stampfer, et al., “Raman intensity mapping of single-walled carbon nanotubes,” *Phys. Rev. B*, vol. 75, p. 041405, 2007.
- [151] Z. Li, J. Ding, P. Finnie, et al., “Raman microscopy mapping for the purity assessment of chirality enriched carbon nanotube networks in thin-film transistors,” *Nano Res*, vol. 8, pp. 2179–2187, 2015.
- [152] A. S. Duarte, J. Rehbinder, R. R. Correia, T. Buckup, and M. Motzkus, “Mapping impurity of single-walled carbon nanotubes in bulk samples with multiplex coherent anti-Stokes Raman microscopy,” *Nano Lett.*, vol. 13, pp. 697–702, 2013.
- [153] C. Chen, N. Hayazawa, and S. Kawata, “A 1.7 nm resolution chemical analysis of carbon nanotubes by tip-enhanced Raman imaging in the ambient,” *Nat. Commun.*, vol. 5, p. 3312, 2013.
- [154] T. A. Yano, T. Ichimura, S. Kuwahara, et al., “Tip-enhanced nano-Raman analytical imaging of locally induced strain distribution in carbon nanotubes,” *Nat. Commun.*, vol. 4, p. 2592, 2013.
- [155] G. G. Hoffmann, O. A. Bârsan, L. G. J. van der Ven, and G. de With, “Tip-enhanced Raman mapping of single-walled carbon nanotube networks in conductive composite materials,” *J. Raman Spectrosc.*, vol. 48, pp. 191–196, 2017.
- [156] B. Lu, C. Zou, Q. Huang, et al., “Widely wavelength-tunable mode-locked fiber laser based on a 45°-tilted fiber grating and polarization maintaining fiber,” *J. Lightwave Technol.*, vol. 37, pp. 3571–3578, 2019.
- [157] C. Zou, T. Wang, Z. Yan, et al., “Wavelength-tunable passively mode-locked Erbium-doped fiber laser based on carbon nanotube and a 45 tilted fiber grating,” *Opt. Commun.*, vol. 406, pp. 151–157, 2018.
- [158] N. Saidin, D. Zen, S. Damanhuri, et al., “Self-starting harmonic mode-locked Tm-Bi co-doped germanate fiber laser with carbon nanotube-based saturable absorber,” *Chin. Opt. Lett.*, vol. 11, p. 063201, 2013.
- [159] M. Nakazawa, S. Nakahara, T. Hirooka, et al., “Polymer saturable absorber materials in the 1.5 μm band using poly-methyl-methacrylate and polystyrene with single-wall carbon nanotubes and their application to a femtosecond laser,” *Opt. Lett.*, vol. 31, pp. 915–917, 2006.
- [160] L. Gui, X. Xiao, and C. Yang, “Observation of various bound solitons in a carbon-nanotube-based erbium fiber laser,” *J. Opt. Soc. Am. B*, vol. 30, pp. 158–164, 2013.
- [161] N. Nishizawa, Y. Seno, K. Sumimura, et al., “All-polarization-maintaining Er-doped ultrashort-pulse fiber laser using carbon nanotube saturable absorber,” *Opt. Express*, vol. 16, pp. 9429–9435, 2008.
- [162] X. Zhao, Z. Zheng, L. Liu, et al., “Switchable, dual-wavelength passively mode-locked ultrafast fiber laser based on a single-wall carbon nanotube modelocker and intracavity loss tuning,” *Opt. Express*, vol. 19, pp. 1168–1173, 2011.
- [163] A. Martinez, S. Uchida, Y.-W. Song, T. Ishigure, and S. Yamashita, “Fabrication of Carbon nanotube-poly-methyl-methacrylate composites for nonlinear photonic devices,” *Opt. Express*, vol. 16, pp. 11337–11343, 2008.
- [164] Y. Zhang, V. Petrov, U. Griebner, et al., “90-fs diode-pumped Yb: CLNGG laser mode-locked using single-walled carbon nanotube saturable absorber,” *Opt. Express*, vol. 22, pp. 5635–5640, 2014.
- [165] M. Chernysheva, A. Krylov, P. Kryukov, et al., “Thulium-doped mode-locked all-fiber laser based on NALM and carbon nanotube saturable absorber,” *Opt. Express*, vol. 20, pp. B124–B130, 2012.
- [166] M. Chernysheva, A. Krylov, A. Ogleznev, et al., “Transform-limited pulse generation in normal cavity dispersion erbium doped single-walled carbon nanotubes mode-locked fiber ring laser,” *Opt. Express*, vol. 20, pp. 23994–24001, 2012.
- [167] F. Wang, A. Rozhin, V. Scardaci, et al., “Wideband-tuneable, nanotube mode-locked, fibre laser,” *Nat. Nanotechnol.*, vol. 3, p. 738, 2008.
- [168] S. Beecher, R. Thomson, N. Psaila, et al., “320 fs pulse generation from an ultrafast laser inscribed waveguide laser mode-locked by a nanotube saturable absorber,” *Appl. Phys. Lett.*, vol. 97, p. 111114, 2010.
- [169] K. Kashiwagi, S. Yamashita, and S. Y. Set, “In-situ monitoring of optical deposition of carbon nanotubes onto fiber end,” *Opt. Express*, vol. 17, pp. 5711–5715, 2009.
- [170] J. Nicholson, R. Windeler, and D. DiGiovanni, “Optically driven deposition of single-walled carbon-nanotube saturable absorbers on optical fiber end-faces,” *Opt. Express*, vol. 15, pp. 9176–9183, 2007.
- [171] Y.-W. Song, S. Yamashita, and S. Maruyama, “Single-walled carbon nanotubes for high-energy optical pulse formation,” *Appl. Phys. Lett.*, vol. 92, p. 021115, 2008.
- [172] Y.-W. Song, S. Yamashita, C. S. Goh, and S. Y. Set, “Carbon nanotube mode lockers with enhanced nonlinearity via evanescent field interaction in D-shaped fibers,” *Opt. Lett.*, vol. 32, pp. 148–150, 2007.
- [173] C. Kim, S. Bae, K. Kieu, and J. Kim, “Sub-femtosecond timing jitter, all-fiber, CNT-mode-locked Er-laser at telecom wavelength,” *Opt. Express*, vol. 21, pp. 26533–26541, 2013.
- [174] A. Martinez, M. Al Araiimi, A. Dmitriev, et al., “Low-loss saturable absorbers based on tapered fibers embedded in carbon nanotube/polymer composites,” *APL Photonics*, vol. 2, p. 126103, 2017.
- [175] A. Martinez, K. Zhou, I. Bennion, and S. Yamashita, “Passive mode-locked lasing by injecting a carbon nanotube-solution in

- the core of an optical fiber," *Opt. Express*, vol. 18, pp. 11008–11014, 2010.
- [176] A. Martinez, K. Zhou, I. Bennion, and S. Yamashita, "In-fiber microchannel device filled with a carbon nanotube dispersion for passive mode-lock lasing," *Opt. Express*, vol. 16, pp. 15425–15430, 2008.
- [177] Y. Li, L. Gao, W. Huang, et al., "All-fiber mode-locked laser via short single-wall carbon nanotubes interacting with evanescent wave in photonic crystal fiber," *Opt. Express*, vol. 24, pp. 23450–23458, 2016.
- [178] S. Y. Choi, F. Rotermund, H. Jung, K. Oh, and D.-I. Yeom, "Femtosecond mode-locked fiber laser employing a hollow optical fiber filled with carbon nanotube dispersion as saturable absorber," *Opt. Express*, vol. 17, pp. 21788–21793, 2009.
- [179] Y.-W. Song, K. H. Fong, S. Y. Set, K. Kikuchi, and S. Yamashita, "Carbon nanotube-incorporated sol-gel glass for high-speed modulation of intracavity absorption of fiber lasers," *Opt. Commun.*, vol. 283, pp. 3740–3742, 2010.
- [180] C. Jin, Y. Cui, and X. Liu, "Glass-hosted carbon nanotubes as a saturable absorber for ultrafast laser," in *The European Conference on Lasers and Electro-Optics* (p. ce_p_34), Optical Society of America, 2019.
- [181] J. B. Schlager, P. D. Hale, and D. L. Franzen, "High-sensitivity optical sampling using an erbium-doped fiber laser strobe," *Microw. Opt. Technol. Lett.*, vol. 6, pp. 835–837, 1993.
- [182] H. A. Haus and W. S. Wong, "Solitons in optical communications," *Rev. Mod. Phys.*, vol. 68, p. 423, 1996.
- [183] R. J. Jones and J.-C. Diels, "Stabilization of femtosecond lasers for optical frequency metrology and direct optical to radio frequency synthesis," *Phys. Rev. Lett.*, vol. 86, p. 3288, 2001.
- [184] S. Yamashita, Y. Inoue, K. Hsu, et al., "5-GHz pulsed fiber Fabry-Pe/spl acute/rot laser mode-locked using carbon nanotubes," *IEEE Photonics Technol. Lett.*, vol. 17, pp. 750–752, 2005.
- [185] A. Grudinin and S. Gray, "Passive harmonic mode locking in soliton fiber lasers," *J. Opt. Soc. Am. B*, vol. 14, pp. 144–154, 1997.
- [186] Y.-W. Song, S. Yamashita, C. S. Goh, and S. Y. Set, "Passively mode-locked lasers with 17.2-GHz fundamental-mode repetition rate pulsed by carbon nanotubes," *Opt. Lett.*, vol. 32, pp. 430–432, 2007.
- [187] S. Yamashita, "Carbon nanotube based mode-locked fiber lasers," in *Asia Optical Fiber Communication and Optoelectronic Exposition and Conference*, Optical Society of America, 2008, p. SaG5.
- [188] H. Yang, A. Wang, and Z. Zhang, "Efficient femtosecond pulse generation in an all-normal-dispersion Yb: fiber ring laser at 605 MHz repetition rate," *Opt. Lett.*, vol. 37, pp. 954–956, 2012.
- [189] J. W. Nicholson and D. J. DiGiovanni, "High-repetition-frequency low-noise fiber ring lasers mode-locked with carbon nanotubes," *IEEE Photonics Technol. Lett.*, vol. 20, pp. 2123–2125, 2008.
- [190] J. Sotor, G. Sobon, J. Jagiello, L. Lipinska, and K. Abramski, "Repetition frequency scaling of an all-polarization maintaining erbium-doped mode-locked fiber laser based on carbon nanotubes saturable absorber," *J. Appl. Phys.*, vol. 117, p. 133103, 2015.
- [191] A. Martinez and S. Yamashita, "Multi-gigahertz repetition rate passively modelocked fiber lasers using carbon nanotubes," *Opt. Express*, vol. 19, pp. 6155–6163, 2011.
- [192] Z. Zhang, L. Zhan, X. Yang, S. Luo, and Y. Xia, "Passive harmonically mode-locked erbium-doped fiber laser with scalable repetition rate up to 1.2 GHz," *Laser Phys. Lett.*, vol. 4, p. 592, 2007.
- [193] A. Grudinin, D. Richardson, and D. Payne, "Passive harmonic modelocking of a fibre soliton ring laser," *Electron. Lett.*, vol. 29, pp. 1860–1861, 1993.
- [194] C. S. Jun, J. H. Im, S. H. Yoo, et al., "Low noise GHz passive harmonic mode-locking of soliton fiber laser using evanescent wave interaction with carbon nanotubes," *Opt. Express*, vol. 19, pp. 19775–19780, 2011.
- [195] J. H. Im, S. Y. Choi, F. Rotermund, and D.-I. Yeom, "All-fiber Er-doped dissipative soliton laser based on evanescent field interaction with carbon nanotube saturable absorber," *Opt. Express*, vol. 18, pp. 22141–22146, 2010.
- [196] K. Kashiwagi and S. Yamashita, "Deposition of carbon nanotubes around microfiber via evanescent light," *Opt. Express*, vol. 17, pp. 18364–18370, 2009.
- [197] Y.-W. Song, K. Morimune, S. Y. Set, and S. Yamashita, "Polarization insensitive all-fiber mode-lockers functioned by carbon nanotubes deposited onto tapered fibers," *Appl. Phys. Lett.*, vol. 90, p. 021101, 2007.
- [198] C. S. Jun, S. Y. Choi, F. Rotermund, B. Y. Kim, and D.-I. Yeom, "Toward higher-order passive harmonic mode-locking of a soliton fiber laser," *Opt. Lett.*, vol. 37, pp. 1862–1864, 2012.
- [199] K. Jiang, S. Fu, P. Shum, and C. Lin, "A wavelength-switchable passively harmonically mode-locked fiber laser with low pumping threshold using single-walled carbon nanotubes," *IEEE Photonics Technol. Lett.*, vol. 22, pp. 754–756, 2010.
- [200] C. Mou, R. Arif, A. Rozhin, and S. Turitsyn, "Passively harmonic mode locked erbium doped fiber soliton laser with carbon nanotubes based saturable absorber," *Opt. Mater. Express*, vol. 2, pp. 884–890, 2012.
- [201] Q. Huang, C. Zou, T. Wang, et al., "Passively harmonic mode-locked Er-doped fiber laser At 1.15 GHz by carbon nanotubes film saturable Absorber," in *Asia Communications and Photonics Conference*, IEEE, 2018, pp. 1–3.
- [202] Q. Huang, C. Zou, T. Wang, et al., "Observation of 550 MHz passively harmonic mode-locked pulses at L-band in an Er-doped fiber laser using carbon nanotubes film," *Chin. Phys. B*, vol. 27, p. 094210, 2018.
- [203] Q. Huang, C. Zou, T. Wang, et al., "Influence of average cavity dispersion and spectral bandwidth on passively harmonic mode locked L-band Er-doped fiber laser," *IEEE J. Sel. Top. Quant. Electron.*, vol. 25, pp. 1–8, 2019.
- [204] Q. Huang, Z. Huang, M. Al Araithi, A. Rozhin, and C. Mou, "2.4 GHz L-band passively harmonic mode locked Er-doped fiber laser based on carbon nanotubes film," *IEEE Photonics Technol. Lett.*, vol. 32, pp. 121–124, 2019.
- [205] H. Khashi, S. Sergeev, M. Al-Araithi, et al., "High-frequency vector harmonic mode locking driven by acoustic resonances," *Opt. Lett.*, vol. 44, pp. 5112–5115, 2019.
- [206] S. W. Harun, N. Saidin, D. Zen, et al., "Self-starting harmonic mode-locked thulium-doped fiber laser with carbon nanotubes saturable absorber," *Chin. Phys. Lett.*, vol. 30, p. 094204, 2013.
- [207] D. Chernykh and A. Krylov, "Gyroscopic effect in the bidirectional femtosecond erbium-doped fiber ring laser," in *International Conference on Lasers Optics*, 2014.
- [208] S. Saito, M. Yamanaka, Y. Sakakibara, et al., "All-polarization-maintaining Er-doped dual comb fiber laser using single-wall

- carbon nanotubes,” *Opt. Express*, vol. 27, pp. 17868–17875, 2019.
- [209] R. D. Baker, N. T. Yardimci, Y.-H. Ou, K. Kieu, and M. Jarrahi, “Self-triggered asynchronous optical sampling terahertz spectroscopy using a bidirectional mode-locked fiber laser,” *Sci. Rep.*, vol. 8, pp. 1–8, 2018.
- [210] K. Kieu and M. Mansuripur, “All-fiber bidirectional passively mode-locked ring laser,” *Opt. Lett.*, vol. 33, pp. 64–66, 2008.
- [211] A. Braga, J.-C. Diels, R. Jain, R. Kay, and L. Wang, “Bidirectional mode-locked fiber ring laser using self-regenerative, passively controlled, threshold gating,” *Opt. Lett.*, vol. 35, pp. 2648–2650, 2010.
- [212] C. Ouyang, P. Shum, K. Wu, et al., “Bidirectional passively mode-locked soliton fiber laser with a four-port circulator,” *Opt. Lett.*, vol. 36, pp. 2089–2091, 2011.
- [213] C. Zeng, X. Liu, and L. Yun, “Bidirectional fiber soliton laser mode-locked by single-wall carbon nanotubes,” *Opt. Express*, vol. 21, pp. 18937–18942, 2013.
- [214] Y. Cui and X. Liu, “Graphene and nanotube mode-locked fiber laser emitting dissipative and conventional solitons,” *Opt. Express*, vol. 21, pp. 18969–18974, 2013.
- [215] X. Yao, “Generation of bidirectional stretched pulses in a nanotube-mode-locked fiber laser,” *Appl. Opt.*, vol. 53, pp. 27–31, 2014.
- [216] L. Li, Q. Ruan, R. Yang, L. Zhao, and Z. Luo, “Bidirectional operation of 100 fs bound solitons in an ultra-compact mode-locked fiber laser,” *Opt. Express*, vol. 24, pp. 21020–21026, 2016.
- [217] H. H. Liu and K. K. Chow, “Operation-switchable bidirectional pulsed fiber laser incorporating carbon-nanotube-based saturable Absorber,” *IEEE J. Sel. Top. Quant. Electron.*, vol. 20, pp. 278–282, 2014.
- [218] X. Zhao, Z. Zheng, Y. Liu, G. Hu, and J. Liu, “Dual-wavelength, bidirectional single-wall carbon nanotube mode-locked fiber laser,” *IEEE Photonics Technol. Lett.*, vol. 26, pp. 1722–1725, 2014.
- [219] A. A. Krylov, D. S. Chernykh, N. R. Arutyunyan, et al., “Generation regimes of bidirectional hybridly mode-locked ultrashort pulse erbium-doped all-fiber ring laser with a distributed polarizer,” *Appl. Opt.*, vol. 55, pp. 4201–4209, 2016.
- [220] M. Chernysheva, M. A. Araimi, H. Kbashi, et al., “Isolator-free switchable uni- and bidirectional hybrid mode-locked erbium-doped fiber laser,” *Opt. Express*, vol. 24, pp. 15721–15729, 2016.
- [221] H. Jiang, Y. Wang, S. Y. Set, and S. Yamashita, “Bidirectional mode-locked soliton fiber laser in 2 μ m using CNT saturable Absorber,” in *Advanced Solid State Lasers*, Optical Society of America, 2017, pp. JM5A–21.
- [222] J. Olson, Y. H. Ou, A. Azarm, and K. Kieu, “Bi-directional mode-locked thulium fiber laser as a single-cavity dual-comb source,” *IEEE Photonics Technol. Lett.*, vol. 30, pp. 1772–1775, 2018.
- [223] Y. Li, K. Yin, X. Zhang, et al., “All-fiber bidirectional mode-locked ultrafast fiber laser at 2 μ m,” *IEEE Photonics J.*, vol. 11, pp. 1–8, 2019.
- [224] M. Meier, V. Romano, and T. Feurer, “Material processing with pulsed radially and azimuthally polarized laser radiation,” *Appl. Phys. A*, vol. 86, pp. 329–334, 2007.
- [225] M.-C. Zhong, L. Gong, D. Li, et al., “Optical trapping of core-shell magnetic microparticles by cylindrical vector beams,” *Appl. Phys. Lett.*, vol. 105, p. 181112, 2014.
- [226] H. Wang, L. Shi, B. Lukyanchuk, C. Sheppard, and C. T. Chong, “Creation of a needle of longitudinally polarized light in vacuum using binary optics,” *Nat. Photonics*, vol. 2, pp. 501–505, 2008.
- [227] X. Cai, J. Wang, M. J. Strain, et al., “Integrated compact optical vortex beam emitters,” *Science*, vol. 338, p. 363, 2012.
- [228] Z.-Y. Rong, Y.-J. Han, S.-Z. Wang, and C.-S. Guo, “Generation of arbitrary vector beams with cascaded liquid crystal spatial light modulators,” *Opt. Express*, vol. 22, pp. 1636–1644, 2014.
- [229] D. Pohl, “Operation of a ruby laser in the purely transverse electric mode TE₀₁,” *Appl. Phys. Lett.*, vol. 20, pp. 266–267, 1972.
- [230] M. A. Ahmed, A. Voss, M. M. Vogel, and T. Graf, “Multilayer polarizing grating mirror used for the generation of radial polarization in Yb:YAG thin-disk lasers,” *Opt. Lett.*, vol. 32, pp. 3272–3274, 2007.
- [231] F. Enderli and T. Feurer, “Radially polarized mode-locked Nd:YAG laser,” *Opt. Lett.*, vol. 34, pp. 2030–2032, 2009.
- [232] T. Grosjean, D. Courjon, and M. Spajer, “An all-fiber device for generating radially and other polarized light beams,” *Opt. Commun.*, vol. 203, pp. 1–5, 2002.
- [233] R. Zheng, C. Gu, A. Wang, L. Xu, and H. Ming, “An all-fiber laser generating cylindrical vector beam,” *Opt. Express*, vol. 18, pp. 10834–10838, 2010.
- [234] B. Sun, A. Wang, L. Xu, et al., “Low-threshold single-wavelength all-fiber laser generating cylindrical vector beams using a few-mode fiber Bragg grating,” *Opt. Lett.*, vol. 37, pp. 464–466, 2012.
- [235] B. Sun, A. Wang, C. Gu, et al., “Mode-locked all-fiber laser producing radially polarized rectangular pulses,” *Opt. Lett.*, vol. 40, pp. 1691–1694, 2015.
- [236] K. Yan, J. Lin, Y. Zhou, et al., “Bi₂Te₃ based passively Q-switched fiber laser with cylindrical vector beam emission,” *Appl. Opt.*, vol. 55, pp. 3026–3029, 2016.
- [237] Y. Zhou, A. Wang, C. Gu, et al., “Actively mode-locked all fiber laser with cylindrical vector beam output,” *Opt. Lett.*, vol. 41, pp. 548–550, 2016.
- [238] H. Wan, J. Wang, Z. Zhang, et al., “High efficiency mode-locked, cylindrical vector beam fiber laser based on a mode selective coupler,” *Opt. Express*, vol. 25, pp. 11444–11451, 2017.
- [239] Y. Zhou, J. Lin, X. Zhang, et al., “Self-starting passively mode-locked all fiber laser based on carbon nanotubes with radially polarized emission,” *Photonics Res.*, vol. 4, pp. 327–330, 2016.
- [240] D. Mao, T. Feng, W. Zhang, et al., “Ultrafast all-fiber based cylindrical-vector beam laser,” *Appl. Phys. Lett.*, vol. 110, p. 021107, 2017.
- [241] Y. Cai, J. Zhang, C. Wang, L. Zhang, and Z. Zhang, “Carbon nanotube mode-locked fiber laser generating cylindrical vector beams with a two-mode fiber bragg grating,” *Appl. Sci.*, vol. 8, p. 643, 2018.
- [242] T. Wang, F. Wang, F. Shi, et al., “Generation of femtosecond optical vortex beams in All-fiber mode-locked fiber laser using mode selective coupler,” *J. Lightwave Technol.*, vol. 35, pp. 2161–2166, 2017.
- [243] Z. Zhang, Y. Cai, J. Wang, H. Wan, and L. Zhang, “Switchable dual-wavelength cylindrical vector beam generation from a passively mode-locked fiber laser based on carbon nanotubes,” *IEEE J. Sel. Top. Quant. Electron.*, vol. 24, pp. 1–6, 2018.
- [244] D. J. Jones, S. A. Diddams, J. K. Ranka, et al., “Carrier-envelope phase control of femtosecond mode-locked lasers and direct optical frequency synthesis,” *Science*, vol. 288, p. 635, 2000.

- [245] T. Rosenband, D. B. Hume, P. O. Schmidt, et al., “Frequency ratio of Al⁺ and Hg⁺ single-ion optical clocks; metrology at the 17th decimal place,” *Science*, vol. 319, p. 1808, 2008.
- [246] J. Millo, M. Abgrall, M. Lours, et al., “Ultralow noise microwave generation with fiber-based optical frequency comb and application to atomic fountain clock,” *Appl. Phys. Lett.*, vol. 94, p. 141105, 2009.
- [247] F. R. Giorgetta, W. C. Swann, L. C. Sinclair, et al., “Optical two-way time and frequency transfer over free space,” *Nat. Photonics*, vol. 7, pp. 434–438, 2013.
- [248] J. Ye, “Absolute measurement of a long, arbitrary distance to less than an optical fringe,” *Opt. Lett.*, vol. 29, pp. 1153–1155, 2004.
- [249] M. Fujiwara, M. Teshima, J. Kani, et al., “Optical carrier supply module using flattened optical multicarrier generation based on sinusoidal amplitude and phase hybrid modulation,” *J. Lightwave Technol.*, vol. 21, pp. 2705–2714, 2003.
- [250] J. Kim and Y. Song, “Ultralow-noise mode-locked fiber lasers and frequency combs: principles, status, and applications,” *Adv. Opt. Photonics*, vol. 8, pp. 465–540, 2016.
- [251] H. R. Telle, G. Steinmeyer, A. E. Dunlop, et al., “Carrier-envelope offset phase control: A novel concept for absolute optical frequency measurement and ultrashort pulse generation,” *Appl. Phys. B*, vol. 69, pp. 327–332, 1999.
- [252] M. Zimmermann, C. Gohle, R. Holzwarth, T. Udem, and T. W. Hänsch, “Optical clockwork with an offset-free difference-frequency comb: accuracy of sum- and difference-frequency generation,” *Opt. Lett.*, vol. 29, pp. 310–312, 2004.
- [253] J. Lim, K. Knabe, K. A. Tillman, et al., “A phase-stabilized carbon nanotube fiber laser frequency comb,” *Opt. Express*, vol. 17, pp. 14115–14120, 2009.
- [254] T.-H. Wu, K. Kieu, N. Peyghambarian, and R. J. Jones, “Low noise erbium fiber fs frequency comb based on a tapered-fiber carbon nanotube design,” *Opt. Express*, vol. 19, pp. 5313–5318, 2011.
- [255] D. Churin, K. Kieu, R. A. Norwood, and N. Peyghambarian, “Efficient frequency comb generation in the 9- μ m region using compact fiber sources,” *IEEE Photonics Technol. Lett.*, vol. 26, pp. 2271–2274, 2014.
- [256] S. Mehravar, R. A. Norwood, N. Peyghambarian, and K. Kieu, “Real-time dual-comb spectroscopy with a free-running bidirectionally mode-locked fiber laser,” *Appl. Phys. Lett.*, vol. 108, p. 231104, 2016.
- [257] Y. H. Ou, J. Olson, S. Mehravar, et al., “Octave-spanning dual-comb spectroscopy with a free-running bidirectional mode-locked femtosecond fiber laser,” in *Conference on Lasers and Electro-Optics*, Optical Society of America, 2017, pp. SM2L–3.
- [258] S. Schweyer, K. Kieu, P. Putzer, et al., “All-in-Fiber polarization maintaining tapered fiber carbon nanotube erbium frequency comb with an integrated electro-optic modulator,” in *European Conference on Lasers and Electro-Optics and European Quantum Electronics Conference*, Optical Society of America, 2017, p. 1.
- [259] N. Nishizawa, Y. Sakakibara, E. Itoga, and H. Kataura, “Optical frequency comb using polarization maintaining Er-doped ultrashort pulse fiber laser with carbon-nanotube polyimide film,” in *Conference on Lasers and Electro-Optics*, Optical Society of America, 2011, p. JThB125.
- [260] N. Nishizawa, T. Nagaike, M. Aramaki, et al., “Optical frequency comb using dispersion managed Er-doped ultrashort pulse fiber laser using carbon nanotube polyimide film,” in *Conference on Lasers and Electro-Optics Pacific Rim*, Optical Society of America, 2013, p. TuF1_3.
- [261] M. Tsuzuki, L. Jin, M. Yamanaka, et al., “Midinfrared optical frequency comb based on difference frequency generation using high repetition rate Er-doped fiber laser with single wall carbon nanotube film,” *Photonics Res.*, vol. 4, pp. 313–317, 2016.
- [262] H. Togashi, T. Nagaike, L. Jin, et al., “All polarization maintaining optical frequency comb based on Er-doped fiber laser with carbon nanotube,” in *Conference on Lasers and Electro-Optics*, Optical Society of America, 2017, pp. JW2A–60.
- [263] N. Nishizawa, T. Niinomi, Y. Nomura, L. Jin, and Y. Ozeki, “Octave spanning coherent supercontinuum comb generation based on Er-doped fiber lasers and their characterization,” *IEEE J. Sel. Top. Quant. Electron.*, vol. 24, pp. 1–9, 2018.
- [264] N. Ohta, L. Jin, Y. Sakakibara, et al., “Wavelength tunable narrow linewidth comb using soliton self-frequency shift and spectral compression technique,” in *Conference on Lasers and Electro-Optics*, Optical Society of America, 2018, pp. STU4K–5.
- [265] X. Zhao, Z. Zheng, Y. Liu, et al., “High-resolution absolute distance measurement using a dual-wavelength, dual-comb, femtosecond fiber laser,” in *Conference on Lasers and Electro-Optics*, Optical Society of America, 2012, pp. CM2J–4.
- [266] X. Zhao, T. Li, Y. Liu, Q. Li, and Z. Zheng, “Polarization-multiplexed, dual-comb all-fiber mode-locked laser,” *Photonics Res.*, vol. 6, pp. 853–857, 2018.
- [267] T. Li, X. Zhao, J. Chen, et al., “Tri-comb and quad-comb generation based on a multi-dimensional multiplexed mode-locked laser,” *J. Lightwave Technol.*, vol. 37, pp. 5178–5184, 2019.
- [268] A. Komarov and F. Sanchez, “Structural dissipative solitons in passive mode-locked fiber lasers,” *Phys. Rev. E*, vol. 77, p. 066201, 2008.
- [269] K. Krupa, K. Nithyanandan, U. Andral, P. Tchofo-Dinda, and P. Grelu, “Real-time observation of internal motion within ultrafast dissipative optical soliton molecules,” *Phys. Rev. Lett.*, vol. 118, p. 243901, 2017.
- [270] A. F. J. Runge, C. Agueraray, N. G. R. Broderick, and M. Erkintalo, “Coherence and shot-to-shot spectral fluctuations in noise-like ultrafast fiber lasers,” *Opt. Lett.*, vol. 38, pp. 4327–4330, 2013.
- [271] G. Herink, F. Kurtz, B. Jalali, D. R. Solli, and C. Ropers, “Real-time spectral interferometry probes the internal dynamics of femtosecond soliton molecules,” *Science*, vol. 356, pp. 50–54, 2017.
- [272] G. Herink, B. Jalali, C. Ropers, and D. R. Solli, “Resolving the build-up of femtosecond mode-locking with single-shot spectroscopy at 90 MHz frame rate,” *Nat. Photonics*, vol. 10, pp. 321–326, 2016.
- [273] A. Mahjoubfar, D. V. Churkin, S. Barland, et al., “Time stretch and its applications,” *Nat. Photonics*, vol. 11, p. 341, 2017.
- [274] H. Chen, M. Liu, J. Yao, et al., “Soliton booting dynamics in an ultrafast Anomalous dispersion fiber laser,” *IEEE Photonics J.*, vol. 10, pp. 1–9, 2018.
- [275] X. M. Liu and Y. D. Cui, “Revealing the behavior of soliton build-up in a mode-locked laser,” *Adv. photonics*, vol. 1, p. 016003, 2019.

- [276] X. Liu, D. Popa, and N. Akhmediev, “Revealing the transition dynamics from Q switching to mode locking in a soliton laser,” *Phys. Rev. Lett.*, vol. 123, p. 093901, 2019.
- [277] X. Liu, X. Yao, and Y. Cui, “Real-time observation of the buildup of soliton molecules,” *Phys. Rev. Lett.*, vol. 121, p. 023905, 2018.
- [278] X. Liu, X. Han, and Y. Zhang, Observation of Multi-Soliton Asynchronous Buildup Dynamics in All-PM Mode-Locked Lasers, 2019, arXiv preprint arXiv:1905.02333.
- [279] X. Liu and M. Pang, “Revealing the buildup dynamics of harmonic mode-locking states in ultrafast lasers,” *Laser Photonics Rev.*, vol. 13, p. 1800333, 2019.
- [280] M. Liu, A. Luo, Y. Yan, et al., “Successive soliton explosions in an ultrafast fiber laser,” *Opt. Lett.*, vol. 41, pp. 1181–1184, 2016.
- [281] M. Liu, A. Luo, W. Xu, and Z. Luo, “Dissipative rogue waves induced by soliton explosions in an ultrafast fiber laser,” *Opt. Lett.*, vol. 41, pp. 3912–3915, 2016.
- [282] M. Liu, Z. Wei, H. Li, et al., “Visualizing the “invisible” soliton pulsation in an ultrafast laser,” *Laser Photonics Rev.*, vol. 14, p. 1900317, 2020.
- [283] S. Sugavanam, C. Mou, J. Peng, and D. Churkin, “Pulse-to-pulse spectral evolution of breathing bound solitons in a mode-locked fiber laser,” in *Conference on Lasers and Electro-Optics, IEEE*, 2015, pp. 1–2.
- [284] M. Liu, H. Li, A. Luo, et al., “Real-time visualization of soliton molecules with evolving behavior in an ultrafast fiber laser,” *J. Opt.*, vol. 20, p. 034010, 2018.
- [285] L. Huang, Y. Zhang, and X. Liu, “Dynamics of carbon nanotube-based mode-locking fiber lasers,” *Nanophotonics*, vol. 1, pp. 1–31, 2020.
- [286] Y. Jiang, T. Narushima, and H. Okamoto, “Nonlinear optical effects in trapping nanoparticles with femtosecond pulses,” *Nat. Phys.*, vol. 6, pp. 1005–1009, 2010.
- [287] L. Tong, V. D. Miljkovic, and M. Kall, “Alignment, rotation, and spinning of single plasmonic nanoparticles and nanowires using polarization dependent optical forces,” *Nano Lett.*, vol. 10, pp. 268–273, 2010.
- [288] N. Kanda, T. Higuchi, H. Shimizu, et al., “The vectorial control of magnetization by light,” *Nat. Commun.*, vol. 2, p. 362, 2011.
- [289] G. D. VanWiggeren and R. Roy, “Communication with dynamically fluctuating states of light polarization,” *Phys. Rev. Lett.*, vol. 88, p. 097903, 2002.
- [290] M. Virte, K. Panajotov, H. Thienpont, and M. Sciamanna, “Deterministic polarization chaos from a laser diode,” *Nat. Photonics*, vol. 7, pp. 60–65, 2012.
- [291] C. Lecaplain, P. Grellu, and S. Wabnitz, “Dynamics of the transition from polarization disorder to antiphase polarization domains in vector fiber lasers,” *Phys. Rev. A*, vol. 89, p. 063812, 2014.
- [292] D. Y. Tang, G. Q. Xie, H. H. Yu, et al., “Graphene mode-locked femtosecond laser at 2 μm wavelength,” *Opt. Lett.*, vol. 37, p. 2085, 2012.
- [293] M. Han, S. Zhang, X. Li, et al., “Polarization dynamic patterns of vector solitons in a graphene mode-locked fiber laser,” *Opt. Express*, vol. 23, pp. 2424–2435, 2015.
- [294] Y. F. Song, H. Zhang, L. M. Zhao, D. Y. Shen, and D. Y. Tang, “Coexistence and interaction of vector and bound vector solitons in a dispersion-managed fiber laser mode locked by graphene,” *Opt. Express*, vol. 24, pp. 1814–1822, 2016.
- [295] S. V. Sergeyev, C. Mou, E. G. Turitsyna, et al., “Spiral attractor created by vector solitons,” *Light Sci. Appl.*, vol. 3, p. e131, 2014.
- [296] C. Mou, S. Sergeyev, A. Rozhin, and S. Turistyn, “All-fiber polarization locked vector soliton laser using carbon nanotubes,” *Opt. Lett.*, vol. 36, pp. 3831–3833, 2011.
- [297] S. V. Sergeyev, C. Mou, A. Rozhin, and S. K. Turitsyn, “Vector solitons with locked and precessing states of polarization,” *Opt. Express*, vol. 20, pp. 27434–27440, 2012.
- [298] V. Tsaturian, S. V. Sergeyev, C. Mou, et al., “Polarisation dynamics of vector soliton molecules in mode locked fibre laser,” *Sci. Rep.*, vol. 3, p. 3154, 2013.
- [299] C. Mou, S. V. Sergeyev, A. G. Rozhin, and S. K. Turitsyn, “Bound state vector solitons with locked and precessing states of polarization,” *Opt. Express*, vol. 21, pp. 26868–26875, 2013.
- [300] H. Khashi, S. V. Sergeyev, C. Mou, et al., “Bright-dark rogue waves,” *Ann. Phys.*, vol. 530, p. 1700362, 2018.
- [301] H. J. Khashi, S. V. Sergeyev, M. A. Araimi, N. Tarasov, and A. Rozhin, “Vector soliton rain,” *Laser Phys. Lett.*, vol. 16, p. 035103, 2019.
- [302] F. Torrisi, D. Popa, S. Milana, et al., “Stable, surfactant-free graphene–styrene methylmethacrylate composite for ultrafast lasers,” *Adv. Opt. Mater.*, vol. 4, pp. 1088–1097, 2016.
- [303] G. Hu, T. Albrow-Owen, X. Jin, et al., “Black phosphorus ink formulation for inkjet printing of optoelectronics and photonics,” *Nat. Commun.*, vol. 8, pp. 1–10, 2017.
- [304] Y. Gladush, A. A. Mkrtchyan, D. S. Kopylova, et al., “Ionic liquid gated carbon nanotube saturable absorber for switchable pulse generation,” *Nano Lett.*, vol. 19, pp. 5836–5843, 2019.
- [305] X. Xu, J. Zhai, Y. Chen, et al., “Well-aligned single-walled carbon nanotubes for optical pulse generation and laser operation states manipulation,” *Carbon*, vol. 95, pp. 84–90, 2015.
- [306] Y. Song, X. Shi, C. Wu, D. Tang, and H. Zhang, “Recent Progress of study on optical solitons in fiber lasers,” *Appl. Phys. Rev.*, vol. 6, p. 021313, 2019.
- [307] Z. Yu, Y. Wang, X. Zhang, et al., “A 66 fs highly stable single wall carbon nanotube mode locked fiber laser,” *Laser Phys.*, vol. 24, p. 015105, 2013.